Statistics of Local Extremes

Larsen, Gunner Chr.; Bierbooms, W.; Hansen, Kurt Schaldemose

Publication date:
2003

Document Version
Publisher's PDF, also known as Version of record

Risø-R-1220(EN)

Statistics of Local Extremes

Gunner Chr. Larsen, Wim Bierbooms and Kurt S. Hansen

Risø National Laboratory, Roskilde, Denmark
December 2003

Abstract

The gust events described in the IEC-standard are formulated as coherent gusts of an inherent deterministic character, whereas the gusts experienced in real situation are of a stochastic nature with a limited spatial extension. This conceptual difference may cause substantial differences in the load patterns of a wind turbine when a gust event is imposed.

The Newgust method is a rational way of taking wind speed gust situations into account in a design process. A corner stone in the method is a cogent algorithm to embed a wind speed gust of a prescribed appearance in a stochastic wind field [Dragt, 1996]. However, dealing with wind turbine design, not only detailed knowledge on the spatial/time structure of the gust event is required. The probability of occurrence of a gust event with a given wind speed amplitude/magnitude is equally important. This theme is addressed in the present report.

A theoretical expression for the probability density function associated with local extremes of a stochastic process is presented. The expression is basically based on the lower four statistical moments and a bandwidth parameter. The theoretical expression is subsequently verified by comparison with simulated synthetic wave/wind fields as well as with measured wind fields covering a broad range of mean wind speed situations and terrain conditions. The simulated wave fields represents narrow band processes, whereas the wind fields represent broad-banded processes.

The work reported makes part of the project “Modelling of Extreme Gusts for Design Calculations ” (NEWGUST), which is co-funded through JOULEIII on contract no. JOR3-CT98-0239.

ISBN 87-550-2777-6
87-550-2778-4 (Internet)
ISSN 0106-2840

Print: Pitney Bowes management Services Denmark A/S, 2003

Contents

1. Background

The work reported makes part of the project “Modelling of Extreme Gusts for Design Calculations ” (acronym: NewGust), which is co-funded through JOULEIII.

In essence the NewGust method, describes a way to combine a stochastic turbulence field (as presently used for fatigue analysis) and a well defined deterministic gust shape (which can be theoretically derived) in such a way that a realistic extreme gust is obtained. The project approach can be divided into the following steps:

1) Experimental verification of the shape of extreme gusts. From theory it follows that the gust shape resembles the autocorrelation function of turbulence. This will be verified by comparing with shapes extracted from an existing database of wind measurements.
2) Determination of the probability distribution function of extreme gusts from a database of wind measurements and/or from theory (in case wind measurements are not available for a long enough period).
3) Development of an advanced method to determine the dynamic response of a wind turbine to extreme gusts. The advanced method will generate wind time series, which can not, in a statistical sense, be distinguished from natural extreme wind gusts.
4) Implementation of the advanced method in a number of existing design packages.
5) Experimental verification of the predicted loading and response of a wind turbine to extreme gusts.

The present report deals with the second of the tasks described above.

2. Introduction

Verification of the structural integrity of a wind turbine structure involves analyses of fatigue loading as well as extreme loading arising from the environmental wind climate. With the trend of persistently growing turbines, the extreme loading seems to become relatively more important.

The extreme loading to be assessed in an ultimate limit state analyses may result from a number of extreme load events including transient operation (start/stop sequences), faults, and extreme wind events. Examples of extreme wind events are extreme mean wind speeds with a recurrence period of 50 years, extreme wind shear, extreme wind speed gusts and extreme wind direction gusts. The present study addresses extreme wind turbine loading arising only from extreme wind speed gust events.

The extreme wind events explicitly accentuated above are included in the currently available draft of the IEC-standard [IEC 61400-1, 1998] as extreme load conditions that must be considered as ultimate load cases when designing a wind turbine. Within the framework of the IEC-standard, these load situations are defined in terms of two independent site variables - a reference mean wind speed and a characteristic turbulence intensity.

However, the gust events described in the IEC-standard are formulated as coherent gusts of an inherent deterministic character, whereas the gusts experienced in real situation are of a stochastic nature with a limited spatial extension. This conceptual difference may cause substantial differences in the load patterns of a wind turbine when a gust event is imposed [Dragt, 1996]. In order to introduce more realistic load situations of a stochastic nature, the NewGust project has been launched. The aim of this project is to obtain experimentally verified theoretical methods that allow for embedding (qualified) predefined gusts (with a well described probability of occurrence) in the stochastics of the turbulence atmospheric wind field. This is in line with what is the common practice when dealing with the fatigue loading. The investigation is limited to investigation of the longitudinal turbulence component, and consequently no attention is paid to wind direction gusts.

The present report deals with an analysis of the probability of occurrence of a gust event of a given wind speed amplitude/magnitude. A theoretical expression for the probability density function (PDF) associated with *local extremes* of a stochastic process is presented. The expression is basically based on the lower four statistical moments and a bandwidth parameter. The theoretical expression is subsequently verified by comparison with simulated synthetic wave/wind fields as well as with measured wind fields covering a broad range of mean wind speed situations and terrain conditions. The simulated *wave* fields represents narrow band processes, whereas the *wind* fields represent broad-banded processes.

3. Reliability in ultimate loading

A through wind turbine design cycle encompasses, among other load situations, an analysis of the wind turbine structural response due to environmental wind speed gust loading. A rational design procedure requires knowledge to the *distribution* of the structural response caused by such loads both in relation to fatigue considerations and, in particular, in relation to assessment of ultimate loading.

Distribution of the wind turbine structural response, caused by wind speed gust loading, can be estimated through simulation of several realisations of stochastic gusts conditioned on the mean wind speed as well as on the gust magnitude. A subsequent determination of the distribution of the structural response, conditioned only on the mean wind speed, is obtained by convolution of the gust magnitude probability density function with the probability density functions conditioned on the wind speed as well as the gust magnitude. Hence the structural response caused by a wind speed gust with an *arbitrary* amplitude results. The final step is now to derive the distribution of the structural response, caused by wind speed gust loading, by an convolution of the structural response distribution, conditioned on the mean wind speed but related to an arbitrary gust magnitude, with the relevant distribution of the mean wind speed. A through review of this aspect of the NewGust methodology is given in [Bierbooms, 2000].

In the present framework, a wind speed gust is defined as a *local* wind speed extreme. Consequently, determination of the distribution of structural response, caused by wind speed gust loading, requires knowledge to the probability density function of *local wind speed extremes*. A theoretical expression for this probability density function is addressed in Chapter 4, and in Chapter 5 the theoretical expression is verified by comparisons with synthetic stochastic fields and with full scale measured stochastic fields, respectively.

4. Theory

The theory of local extremes has been approached by a thorough literature study and most of the relevant information has been found in general publications on statistics. For *Gaussian* stochastic processes, the statistics of local extremes has been treated by [Cartwright, 1956]. However, the present investigations (cf. Chapter 5), and the analyses of mean gust shapes carried out in [Larsen, 2003], have indicated that for sites with complex oreographic characteristics, *non-Gaussian* wind speed processes may result. The statistics of local extremes, associated with these non-Gaussian stochastic processes, are treated by combining a Hermite polynomial transformation with the local extreme statistics associated with Gaussian processes.

4.1 Gaussian processes

The statistics of local extremes of a Gaussian process was first treated by Rice [Rice, 1944]. However, the theoretical expressions summarised in this section are based on [Cartwright, 1956].

4.1.1 Derivation of the PDF of local extremes

The derivation of the distribution of the local maxima of a Gaussian stochastic process, with an arbitrary bandwidth, is briefly summarised.

A random Gaussian process, f(t), with zero mean can be represented as the sum of an infinite number of cosinus waves as

$$f(t) = \sum_{n=1}^{\infty} c_n \cos(\sigma_n t + \varepsilon_n) \quad , \tag{1}$$

where the frequencies σ_n are distributed densely in the interval $[0;\infty[$, the phases ϵ_n are random and distributed uniformly between $[0;2\pi]$, and the amplitudes c_n are such that in any small interval of frequency $d\sigma$ the following relation holds

$$\sum_{\sigma}^{\sigma+d\sigma} \tfrac{1}{2} c_n^2 = E(\sigma) d\sigma \quad , \tag{2}$$

in which $E(\sigma)$ is the autopower spectral density function (APSD) of *f(t)*.
The n^{th} moment of $E(\sigma)$ is defined as:

$$m_n = \int_0^{\infty} E(\sigma) \sigma^n d\sigma \quad . \tag{3}$$

In order to find the distribution of local maxima of f(t) it is noted that if f(t) has a maximum in the interval [t;t+dt] then, in this interval, the first time derivative of f(t), f'(t), must take values in a range of width closely approximated by |f"(t)|dt , where f"(t) is the second time derivative of f(t). The probability of this occurrence and of f(t) simultaneously lying in the range $[\xi_1;\xi_1 + d\xi_1]$ can be expressed as:

$$\int_{-\infty}^{0} [p(\xi_1, 0, \xi_3) d\xi_1 . |\xi_3| dt] d\xi_3 \quad , \tag{4}$$

where $p(\xi_1, \xi_2, \xi_3)$ is the joint probability of f, f' and f". By utilising the central limit theorem it can be concluded that this joint probability distribution is also normal and can be expressed in terms of the covariance matrix Λ as

$$p(\bar{x}) = \frac{1}{(2\pi)^{n/2} \sqrt{\det(\Lambda)}} e^{-\frac{1}{2} \cdot \bar{x}^T \cdot Q \cdot \bar{x}} \quad , \tag{5}$$

with

$$Q = \Lambda^{-1}. \tag{6}$$

The *mean* frequency, F, of maxima in the range $[\xi_1; \xi_1 + d\xi_1]$ is obtained from (4) and expressed by

$$F(\xi_1) d\xi_1 = \int_{-\infty}^{0} [p(\xi_1, 0, \xi_3) |\xi_3| d\xi_1] d\xi_3 \quad . \tag{7}$$

The probability distribution of local maxima is found by dividing the distribution espressed in (7) by the total mean frequency of maxima N_1 given by

$$N_1 = \int_{-\infty}^{\infty} F(\xi_1) d\xi_1 = \frac{1}{2\pi} \sqrt{\frac{m_4}{m_2}} \quad . \tag{8}$$

Substitution of the expression for the joint Gaussian distribution given in (5) into relation (7) results, after several lengthy manipulations of the involved integrals, in the PDF of the local maxima.

Introducing the normalised local maxima as

$$\eta = \xi_1 / m_0^{\frac{1}{2}} \quad , \tag{9}$$

the requested PDF can be formulated as

$$p(\eta) = \frac{1}{(2\pi)^{1/2}} \left[\delta \cdot e^{-\frac{1}{2}\eta^2/\delta^2} + (1-\delta^2)^{\frac{1}{2}} \eta \cdot e^{-\frac{1}{2}\eta^2} \int_{-\infty}^{\eta(1-\delta^2)^{\frac{1}{2}}/\delta} e^{-\frac{1}{2}x^2} dx \right] , \qquad (10)$$

where the bandwidth parameter, δ, has been introduced. The bandwidth parameter is defined as

$$\delta = \sqrt{\frac{m_0 m_4 - m_2^2}{m_0 m_4}} , \qquad (11)$$

and it will be discussed in more details in section 4.1.2.

The derived PDF of the local maxima, as expressed by (10) and (11), is denoted the Rice distribution. This distribution is described in terms of only one distribution parameter – the bandwidth parameter. For narrow banded stochastic processes the bandwidth parameter approaches zero, and in this limit the PDF will approach a Rayleigh distribution. In case of broad-banded stochastic processes, the band width parameter tend to one, and in this limit expression (10) reduces to a Gaussian distribution. As f(t) is symmetrical about the zero mean level, the PDF of the local minima can be derived directly from relation (10) by replacing η replaced by –η.

4.1.2 The bandwidth parameter

Basically, the band width parameter, δ, is a measure of the width of the spectral density function E(σ). A small value of δ indicates a narrow-banded spectrum; a value of δ close to one corresponds to a broad-banded spectrum. The first asymptotic case ($\delta \rightarrow 0$) yields a distribution of the maxima associated with a stochastic process with an infinitely narrow spectrum. In this case expression (10) simplifies to

$$p(\eta) = \begin{cases} \eta \cdot e^{-\frac{1}{2}\eta^2} & (\eta \geq 0) , \\ 0 & (\eta \leq 0) \end{cases} \qquad (12)$$

which is recognised as the Rayleigh distribution.

The second asymptotic case ($\delta \rightarrow 1$) relates to a broad-banded stochastic signal. In this case the distribution of local extremes degenerates to

$$p(\eta) = \frac{1}{(2\pi)^{\frac{1}{2}}} e^{-\frac{1}{2}\eta^2} , \qquad (13)$$

which is simply a Gaussian distribution (and thus equal to the distribution of the stochastic process itself).

In Figure (4-1) the PDF of local extremes, p(η), is shown for several values of δ. The transition from a Rayleigh to a Gaussian distribution can be clearly seen.

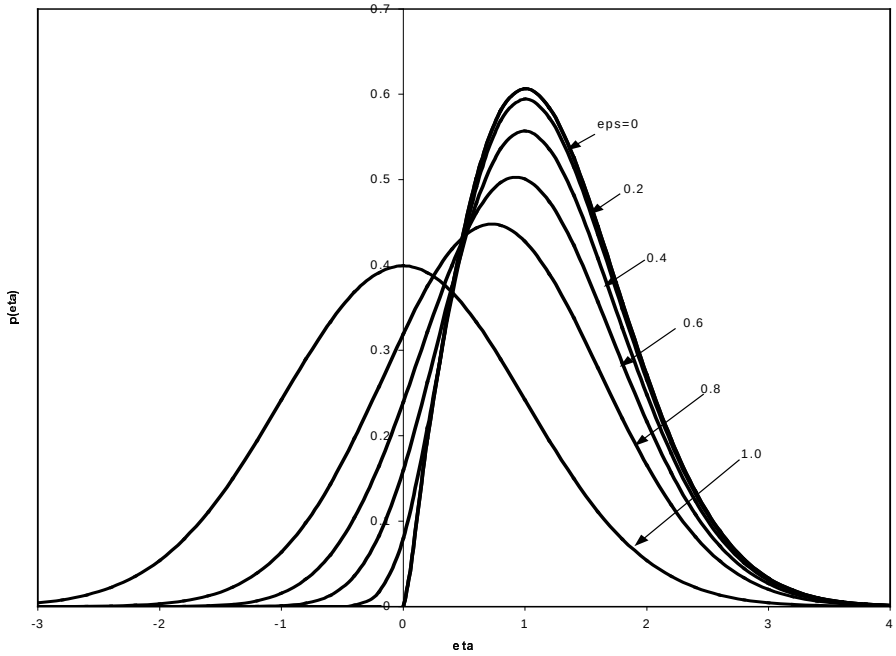

Figure 4-1 The probability density function p(η) of the normalised maximum η illustrated for different values of the bandwidth parameter δ.

In expression (11) the bandwidth parameter has been defined in terms in spectral moments. However, based on geometrical arguments, it is possible to derive an alternative expression for the bandwidth based entirely on quantities that can be obtained directly from a time series representation of the stochastic signal.

Denoting the ratio between the number of negative maxima and the total number of maxima in a given stochastic signal by r, the bandwidth parameter can be expressed as

$$\delta = \sqrt{1-(1-2r)^2} \quad . \tag{14}$$

Another alternative is

$$\delta = \sqrt{1-\gamma^2} \quad , \tag{15}$$

where γ is the ratio between the frequency of zero-upcrossings and the frequency of maxima.

4.2 Non-Gaussian processes

The derivation of expression (10) assumes underlying Gaussian stochastic processes, and this formulation of the PDF for local extremes is thus not applicable to stochastic processes that exhibit a non-Gaussian behaviour. However, for moderate deviations from the Gaussian behaviour (which is usually the case for wind speed measurements), the local extreme PDF, expressed for Gaussian processes in (10), can be transformed to a local extreme PDF associated with a non-Gaussian process by utilising a Hermite moment transformation based on a forth moment Hermite polynomial expansion [Winterstein, 1988]. The Hermite polynomials are orthogonal polynomials, and consequently the involved expansion terms will be statistically uncorrelated.

Mean, variance, skewness and kurtosis of the underlying non-Gaussian stochastic process, X, are denoted by α_1, α_2, α_3 and α_4, respectively. U is a standard Gaussian process.

For $\alpha_4 > 3$, the transformation, H, reads

$$
\begin{aligned}
&X = H(U) = \alpha_1 + \kappa\sqrt{\alpha_2}\left[U + c_3\left(U^2 - 1\right) + c_4\left(U^3 - 3U\right)\right], \\
&c_4 = \frac{\sqrt{1+36h_4}-1}{18}; \quad h_4 = \frac{\alpha_4 - 3}{24}, \\
&c_3 = \frac{h_3}{1+6c_4}; \quad h_3 = \frac{\alpha_3}{6}, \\
&\kappa = \frac{1}{\sqrt{1+2c_3^2+6c_4^2}} \quad .
\end{aligned}
\tag{16}
$$

For $\alpha_4 < 3$, the transformation, H, reads

$$
\begin{aligned}
&X = H(U) = \alpha_1 + \sqrt{\alpha_2}\left[\left(\sqrt{c^2+k}+c\right)^{1/3} - \left(\sqrt{c^2+k}-c\right)^{1/3} - a\right], \\
&c = 1.5b(a+U) - a^3 \quad , \\
&b = -\frac{1}{3h_4}; \quad h_3 = \frac{\alpha_3}{6} \quad , \\
&a = \frac{h_3}{3h_4}; \quad h_4 = \frac{\alpha_4 - 3}{24} \quad , \\
&k = \left(b - 1 - a^2\right)^3 \quad .
\end{aligned}
\tag{17}
$$

When deviation from a Gaussian behaviour is observed for a wind speed signal, the distribution tails is usually more dominant than compared to a Gaussian distribution, and consequently the kurtosis for such signals will usually be larger than 3. However, also examples of kurtosis values less than 3 can be observed.

As seen the transformation is monotonous, which in particular implies that local extremes in the Gaussian process U are transformed to local extremes in the non-Gaussian process X. Thus, the probability that the local extreme, u, associated a Gaussian process is less that U, $\text{PROB}_G(U<u)$, must equal the probability that the local extreme, X = H(U), associated the non- Gaussian process is less that H(u), $\text{PROB}_{nG}(X<H(u))$. Expressing this identity in terms of the cumulative distribution functions (CDF) for local extremes related to the Gaussian and to the non-Gaussian underlying stochastic process, respectively, we obtain

$$
P_G(u) = P_{nG}(H(u)) \quad , \tag{18}
$$

where P_G and P_{nG} denote the CDF's associated with the Gaussian and the non-Gaussian underlying processes. The probability density distributions for the normalised local extremes is thus related according to

$$
p_{nG}(H(\eta)) = \frac{p_G(\eta)}{H'(\eta)} \quad , \tag{19}
$$

where p_G denotes the PDF (related to an underlying Gaussian process) expressed by relation (10), and p_{nG} denotes the PDF related to a underlying non-Gaussian process. The prime denotes derivative with respect to the variable η.

An alternative, and maybe more straight forward formulation, is

$$p_{nG}(\eta) = \frac{p_G\left(H^{-1}(\eta)\right)}{H'\left(H^{-1}(\eta)\right)} \quad . \tag{20}$$

5. Verification

The present chapter deals with a verification of the theoretical model for the *local* extreme statistics as presented in Chapter 4. The verification is performed by comparing model predictions to analysis of both wave/wind simulations and of full-scale wind field measurements. The synthetic stochastic processes encompass both narrow banded stochastic processes (wave simulations) and broad-banded stochastic processes (wind simulations). All synthetic processes were ideal Gaussian processes. The full-scale stochastic processes were represented by (broad-banded) wind measurements. Both Gaussian and non-Gaussian processes have been analysed.

5.1 Narrow banded synthetic signals

The distribution of (local) extremes of a narrow-banded Gaussian stochastic signal is a Rayleigh distribution. This has been experimentally verified for heights of sea waves, and as a result the Rayleigh distribution has been used for fatigue analysis in the frequency domain, thus replacing the Rainflow Counting method traditionally used in the time domain.

The present investigation concerns an analysis of the distribution of local extremes in a narrow banded synthetic Gaussian stochastic signal. The analysed signal examples relate to simulations of Gaussian stochastic wave heights. Assuming a Pierson Moskowitz wave spectrum, a stochastic wave signal can be generated applying the common Shinozuka method (which forms the basis of many stochastic wind field generators).

An example of (a part of) a generated stochastic wave signal is shown in Figure (5-1). Figure (5-2) shows the associated estimated spectrum (using a standard Matlab routine, based on the Welch method) compared to the Pierson Moskowitz spectrum, which is used as target spectrum for the stochastic simulation.

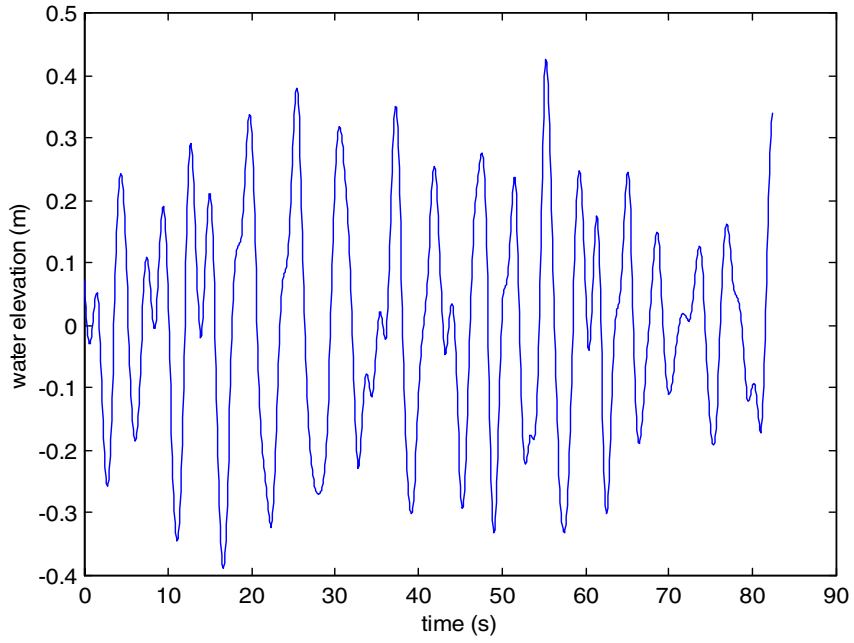

Figure 5-1 Example of a stochastic wave signal (Hs=0.75 m and Tz= 3.5 s).

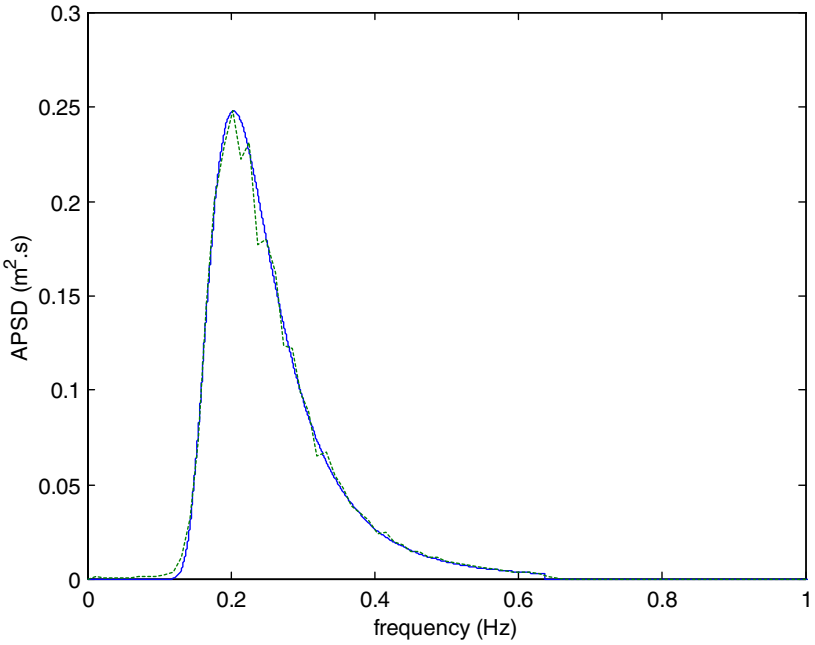

Figure 5-2 Comparison of theoretical spectrum (solid line) and estimate spectrum (dashed line) associated with the wave signal presented in Figure (5-1) (Hs=0.75 m and Tz= 3.5 s).

A total of five realisations have been generated for two sea states:

- significant wave height H_s=0.75m and zero crossing period T_z=3.5s; and
- significant wave height H_s=4.75m and zero crossing period T_z=6.5s .

The spectra are truncated at 0.64 Hz (4 rad/s). The length of each simulation is 3 hours (corresponding to a sea state), and a sampling rate of about 12 Hz has been used. In total 131,072 time points are generated.

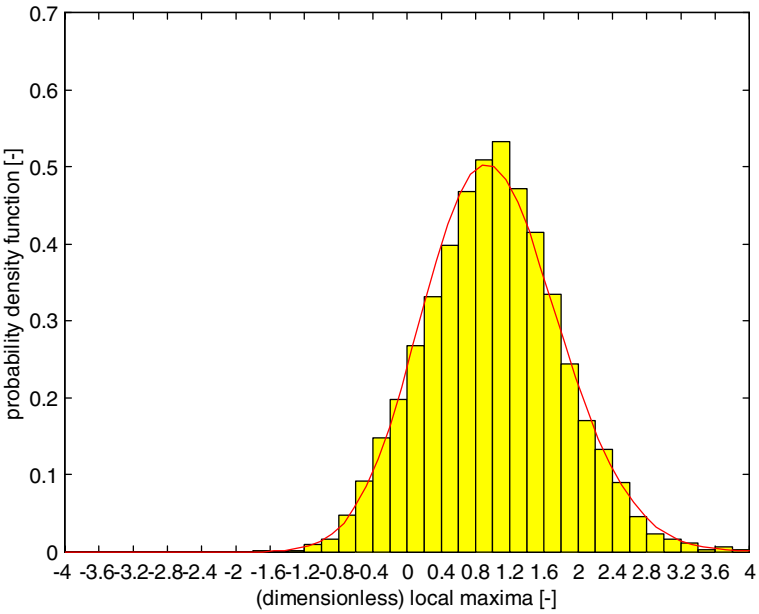

Figure 5-3 PDF's derived from synthetic signal (histogram) compared to theory.

The histogram representation of the distribution of local (normalised) maxima, originating from the generated five time series, is shown in Figure (5-3) together with the theoretical distribution determined according to equation (10). The agreement is excellent.

The applied bandwidth (for the theoretical curves) is derived from equation (11). The involved spectral moments are determined from the expression of the applied spectrum (Pierson Moskowitz) with the aid of the formula manipulation package Maple.

The bandwidth parameter, as well as the (mean) frequency of maxima expressed in equation (8), is given in Table (5-1). For the sake of completeness, also the frequency of the zero-upcrossings ($1/(2*\pi)$. m_2/m_0) is given. The bandwidth values, determined from the time signals applying equation (14), agree perfectly with the theoretical ones.

	Theoretical	Analysis
bandwidth [-]	0.600	0.60 ± 0.01
frequency of zero-upcrossings [Hz]	0.269	0.268 ± 0.002
frequency of local maxima [Hz]	0.336	0.335 ± 0.001

Table 5-1 Statistical parameters associated with the sea state Hs=0.75 m and Tz=3.5 s; comparison between theoretical values and values determined from the generated stochastic time series.

A similar analysis have been performed for the (heavy) sea state defined by H_s=4.75 m and T_z=6.5 s. The results are presented in Figure (5-4) and in Table 2, respectively. The agreement between the theoretical results and the results obtained from a data analysis is again excellent.

	Theoretical	Analysis
bandwidth [-]	0.730	0.73 ± 0.02
frequency of zero-upcrossings [Hz]	0.151	0.150 ± 0.001
frequency of local maxima [Hz]	0.221	0.221 ± 0.001

Table 5-2 Statistical parameters associated with the sea state Hs=4.75 m and Tz=6.5 s; comparison between theoretical values and values determined from the generated stochastic time series.

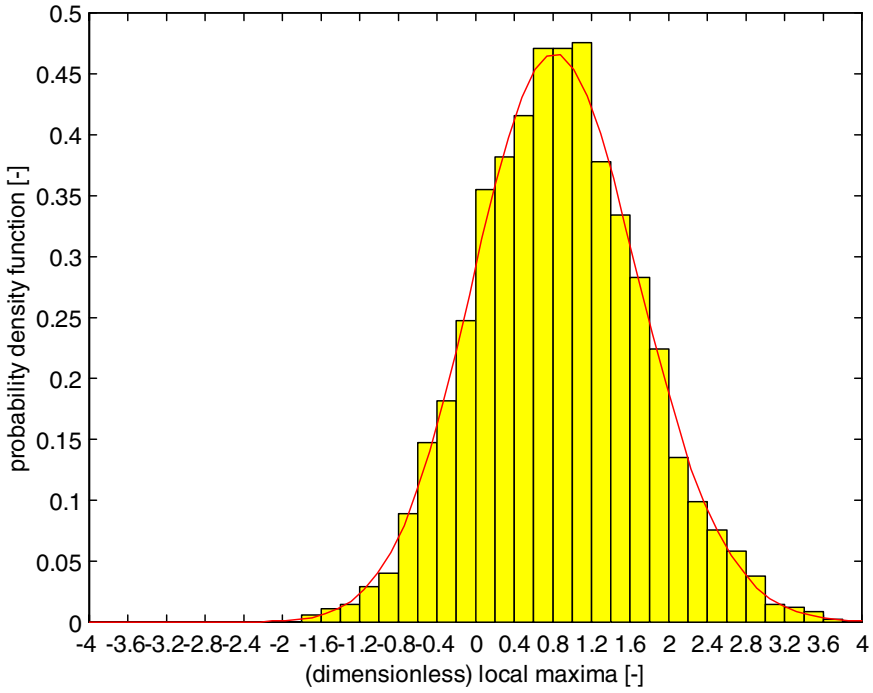

Figure 5-4 PDF's derived from synthetic signal (histogram) compared to theory (Hs=4.74m and Tz=6.5s).

5.2 Broad-banded synthetic signals

In this subsection synthetic turbulence is analysed. This type of stochastic signal is much more broad-banded than the type of stochastic signal associated with wave heights.

Using the wind field simulation package SWING4 [Bierbooms, 1998], wind speed time series are generated for two mean wind speeds (10 m/s and 20 m/s) and for three altitudes (35m, 40m and 80m). SWING4 is capable of generating all three turbulence components of a wind field. A special feature of SWING4 is that the wind velocities are calculated only at desired points on the (rotating) blades instead of at some fixed points in the rotor plane. SWING4 is fully compatible with the commonly applied standards for wind turbine design (IEC, GL and Danish Standard).

SWING4 is based on the energy spectrum of von Karman in combination with the commonly applied Taylor's frozen turbulence hypothesis. This corresponds to the von Karman isotropic turbulence model as specified in the IEC-standard for wind turbine load calculations. The application of the energy spectrum of von Karman implies that implicitly all coherences (C_{uu}, C_{vv}, C_{ww}, C_{uv}, C_{uw} and C_{vw}, where u denotes the longitudinal, v the lateral and w the vertical velocity component) are included in a consistent way. This can not be achieved applying other theoretical or measured spectra and coherence functions. Although SWING4 is based on the isotropic turbulence theory, the method is adopted in such a way that other spectra (from theory or from measurements) can be used (e.g. the spectra given in the IEC and Danish Standard).

For the present investigation, only the longitudinal component of the generated wind field will be used. The isotropic turbulence model has been chosen, i.e. the von Karman spectrum and the corresponding coherence functions, which may be expressed in modified

Bessel functions of the 2nd kind. In order to obtain the stochastic wind field in a fixed frame of reference, the rotational speed (of a hypothetical wind turbine) has been specified to a very low value. The generated wind fields have been extensively tested to ensure that the required spectra are achieved in the simulations.

In order to generate a sufficient amount of gusts for each mean wind speed (bin), 100 wind field realisations have been generated, each of a duration of more than 10 minutes and with a high sampling rate (i.e. 16384 time steps with a time separation equal to 0.04 s). For the analysis described here the same 100 wind fields are applied as for the analysis of the mean gust shape, which formed the first work package of the *New*Gust project [Larsen, 2003].

In Table (5-3), the statistical parameters, associated with the turbulence fields with a mean wind speed equal to 10 m/s, are presented. Table (5-4) presents the analogue statistics for the 20 m/s mean wind speed case. The theoretical bandwidth parameter is evaluated for a maximum frequency of 12.5 Hz (corresponding to a time step equal to 0.04 s) based on the expression for the von Karman spectrum.

Note: The empirical values for the frequency of zero-upcrossings and the local maxima are small compared to the theoretical ones. This is not related to the use of SWING4, but is due to the fact that the efficient FFT (Fast Fourier Transform) is used (which is standard for stochastic generators based on the Shinozuka method) instead of a direct summation of cosinus functions (cf. equation (1)). A consequence of this is, that the time steps are directly related to the frequency steps involved; the time step is just small enough to show the highest frequency involved. This is illustrated in Figure (5-5). The line with circles shows some stochastic signal with a high sampling rate (e.g. determined through summation of cosinus functions, so any time instant can be evaluated). The line with asterisks represents a lower sampling rate corresponding to the application of a FFT algorithm. Although all necessary information is available, the function is, using the FFT, not evaluated at more time points than indicated by the asterisks. Due to the low sampling rate (and the linearisation), the zero-upcrossing just after t=36.9s is missing. A similar explanation can be given for the frequency of local maxima. Notice that this phenomenon has no effect on the applicability of such stochastic wind fields for a fatigue analysis; the maximum frequency, for the wind field generation, is set (much) higher than the highest natural frequency of the wind turbine which is of interest for a dynamic simulation.

	Theoretical	Analysis
bandwidth [-]	0.995	0.993 ± 0.001
frequency of zero-upcrossings [Hz]	0.827	0.725 ± 0.006
frequency of local maxima [Hz]	7.91	6.17 ± 0.02

Table 5-3 Statistical parameters associated with mean wind speed V=10 m/s (at height 40 m); comparison between the theoretical values and values determined from the generated stochastic time series.

	Theoretical	Analysis
bandwidth [-]	0.991	0.989 ± 0.001
frequency of zero-upcrossings [Hz]	1.05	0.903 ± 0.008
frequency of local maxima [Hz]	7.91	6.22 ± 0.02

Table 5-4 Statistical parameters associated with mean wind speed V=20 m/s (at height 40 m); comparison between the theoretical values and values determined from the generated stochastic time series.

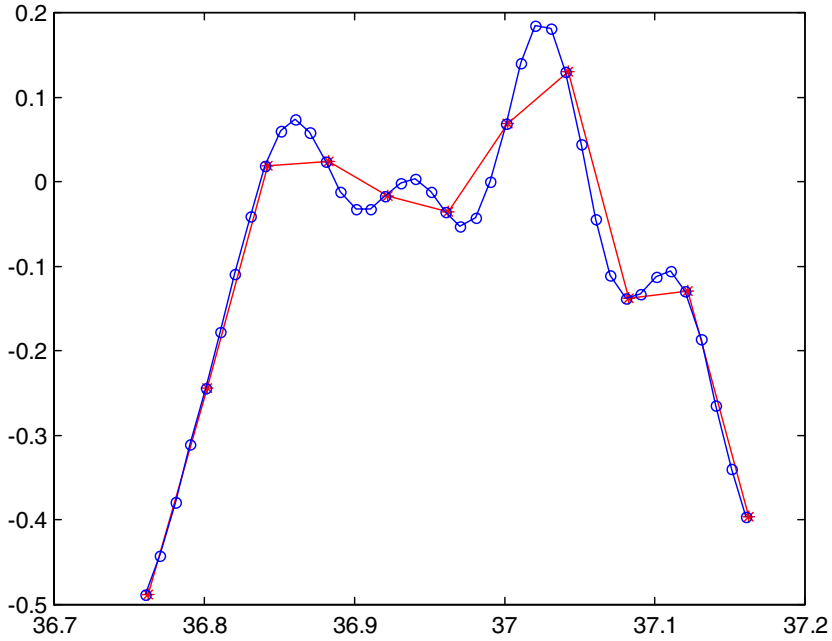

Figure 5-5 Comparison of a stochastic time series associated with high (circles) and low (asterisks) sampling rate.

The histogram representing the distribution of local maxima, for a mean wind speed equal to 10 m/s, are shown in Figure (5-6). The agreement with the theoretical is again very good.
The results for a mean wind speed equal to 20 m/s are presented in Figure (5-7). The difference in the bandwidth is small between the signals related to the mean wind speeds 10 m/s and 20 m/s, respectively. Therefore, there is hardly any difference between the distributions of the extremes for these two mean wind speeds.

It has further been verified that the generated wind speed time series associated with the other two heights (35m and 80m) resulted in the same distributions. These results are not shown here.

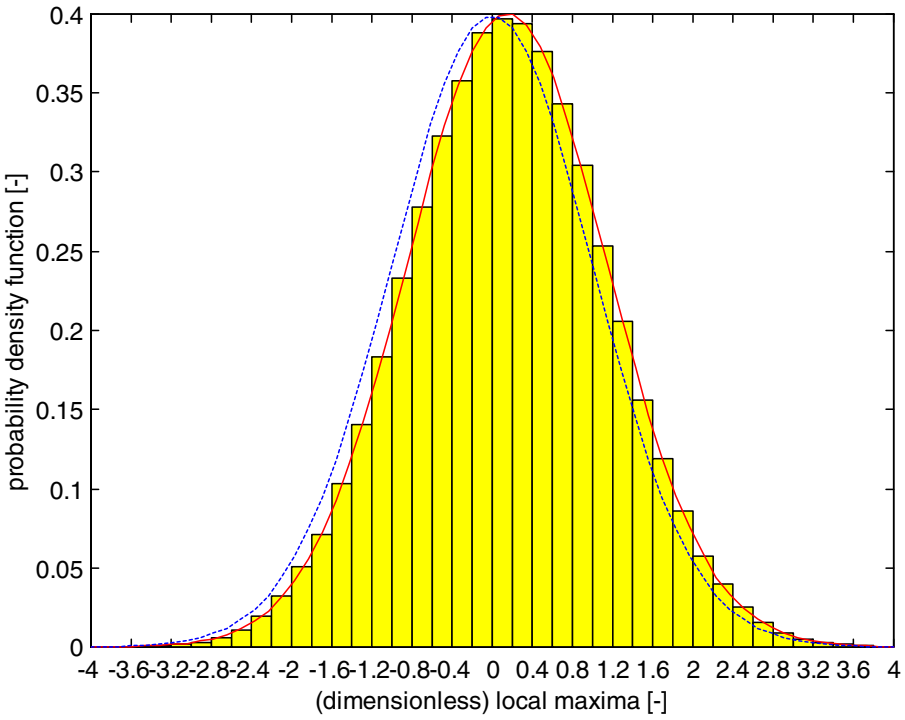

Figure 5-6 PDF's derived from synthetic signal (histogram) compared to theory (V=10m/s).

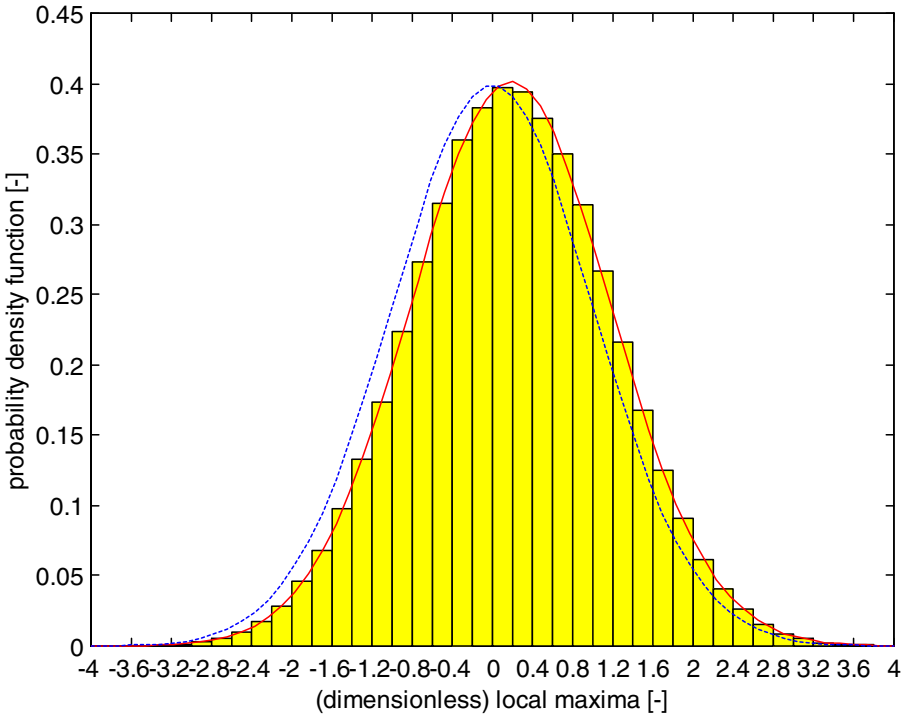

Figure 5-7 PDF's derived from synthetic signal (histogram) compared to theory (V=20m/s).

5.3 Broad-banded measured signals

In addition to *simulated* wave- and turbulence fields, the theoretical extreme distribution is verified against (full-scale) *measurements*. The applied wind speed measurements are available from "Database on Wind Characteristics" (http://www.winddata.com/) - a huge WEB-database covering a vast amount of wind data measured at many different locations.

In analogy with the investigation of the mean gust shapes in [Larsen, 2003], four different terrain conditions are considered - a shallow water off-shore site, a flat coastal region, a flat and homogeneous inland terrain and a complex (mountainous) high wind site.

5.3.1 Data material

It has been the intention to investigate a variety of different terrain types in order to make the analysis as "terrain independent" as possible. The particular choice of sites is in addition guided by considerations concerning amount of data, height of wind speed sensors above terrain, number of wind speed sensors and their mutual position, wind speed sample frequency, mean wind speed range and data quality.

Four different terrain categories are investigated. These represent a shallow water offshore site, a flat coastal region, a flat and homogeneous inland terrain and a complex (mountainous) high wind site. The (shallow water) *offshore* terrain class is characterised by having open sea upstream conditions. The *coastal* terrain class encompasses flat coastal regions with water as well as land as upstream conditions. The upstream conditions for the *flat and homogeneous* terrain type is characterised by flat agricultural land and the *mountainous* terrain is characterised by sharp terrain contours where flow separation is likely to take place. Each of the selected sites represents a substantial amount of data ranging between 2910 and 4470 10-minute time series.

The four selected sites and the associated measuring system are described in details in the following.

Cabauw:

The Cabauw site is a Dutch site representing flat and homogeneous terrain conditions. A large meteorological tower is erected at the site. The meteorological mast is a tubular tower with a height of 213m and a diameter of 2m. Guy wires are attached at four levels. From 20m upwards horizontal trussed measurements booms are installed at intervals of 20m. At each level there are three booms, extending 10.4m from the centre line of the tower. These booms point to the directions 10, 130, 250 degrees relative to North. The SW and N booms are used for wind velocity and wind direction measurements. These booms carry at the end two lateral extensions with a length of 1.5m and a diameter of about 0.04m.

The available amount of data consists of 2910 10-minute wind speed time series recorded from cup anemometers at levels 40m and 80m with a sample frequency of 2Hz. Only the recordings taken at level 80m are used in the present investigation. The mean wind speeds range between 4m/s and 23m/s and mean turbulence intensity is 11.4% with a clear trend of decreasing scatter around the mean value with increasing mean wind speed. This observation is expected as the thermal contribution to the turbulence generation generally tend to diminish for increasing mean wind speed such that the atmospheric stability for high mean wind speeds approach the neutral regime.

The statistics of the wind speed turbulence was investigated in [Larsen, 2003], and at this site the wind speed process was demonstrated to be close to a Gaussian process, at least in a "average" sense when evaluated in terms of the third and forth order statistical moment.

Vindeby:

The world's first offshore wind farm is located on a shallow water area off the north-western coast of the island of Lolland, close to Vindeby in Denmark. The wind farm consists of 11 wind turbines positioned in two rows oriented approximately in a NW-SE direction. The most southerly placed wind turbine is closest to the coast, and the distance is approximately 1.5 km.

In order to investigate the offshore- and coastal wind climate three 45m high meteorological towers were erected at the site. Two of these were located *offshore* and they are denoted by SMW (sea mast west) and SMS (sea mast south), respectively. The perpendicular distance between the western mast and the western wind turbine row was 300m. SMS is located 300m south of the most southern placed turbine. The third mast was erected on land nearly 1.5 km south of the off-shore wind farm a very *flat coastal area*. The land mast is denoted by LM, and its distance to the coast line is approximately 16 m.

The instrumentation of the meteorological towers included sensors at multiple levels. Basically, similar instruments on each of the three masts have been installed in roughly the same level relative to the mean sea level. The monitoring sample rate (for the sensors relevant for this investigation) was 5Hz, and the data was reduced and stored as half-hourly means supplemented with representative time series covering roughly 10% of the total monitoring period.

The intensive measuring campaigns cover two periods. The intensive campaign in the fall of 1994 includes data for Julian days 276 through 311, or October 3rd to November 7th. The intensive campaign in the spring of 1994 includes data for Julian days 118 through 125, or April 28th to May 5th.

The Vindeby site was used to represent both offshore and coastal terrain conditions. The off-shore conditions are extracted from the SMS recordings by restricting the available data recordings to records representing mean wind directions between 226 degrees and 339 degrees (north equals zero degrees) such that in wake effects from the wind turbines are avoided. The coastal conditions are obtained from the LM recordings restricting the data material to recordings with mean wind direction ranging between 67 degrees and 251 degrees.

The available amount of data describing the *offshore* situation consists of 4188 10-minute wind speed time series recorded from cup anemometers positioned at levels 48m, 43m and 38m. Only data from the 48m level are used in the present study. The mean turbulence intensity (for all mean wind speeds) is 6% with a standard deviation equal to 1.9%.

The available amount of data describing the *coastal* situation consists of 3576 10-minute wind speed time series recorded from cup anemometers positioned at levels 46m, 38m and 20m. Only data from the 46m level are used in the present study. The mean wind speeds range in size from 5m/s to 21m/s, and the mean turbulence intensity (for all available mean wind speeds) is 10.3% with a standard deviation of 3.2%.

The statistics of the wind speed turbulence was investigated in [Larsen, 2003], and the wind speed process was demonstrated to be close to a Gaussian process, at least in a “average” sense when evaluated in terms of the third and forth order statistical moment.

Oak Creek:

Wind field measurements is currently being performed in a wind farm situated at a high wind (mountainous) site in Oak Creek, near Tehachapi in California. The measuring campaign is planned to continue during a one and a half-year period, and at present data for a half-year period are available. The purpose of the measurements is to gain knowledge of wind turbine loads caused by extreme wind load conditions.

The wind field is measured from two 80m high meteorological towers erected at a ridge in the terrain. The distance between the two towers is 25.5m. The meteorological towers are instrumented at several heights with both sonics and cup anemometers. Basically, similar instruments on each of the two masts are installed in roughly the same level relative to the terrain level.

The monitoring system is running continuously, and the data are reduced and stored as 10-minutes statistics supplemented with intensive time series recordings covering periods where the mean wind speed exceeds a specified threshold (15 m/s) or the wind turbines operate in a transient load situation. The monitoring sample rate is 8Hz for the signals of relevance for the present investigation.

In the present analysis, the cup anemometer wind speeds recorded at the level 79m on mast 1 are used. The available amount of data describing the *mountainous* terrain conditions consists of 4470 10-minute wind speed time series. The mean wind speeds range between 5m/s and 28m/s with the bulk of the data in the high wind regime above 15m/s. The mean turbulence intensity is 8.6% with a standard deviation equal to 4.6%.

For the Oak Creek site, the investigation in [Larsen, 2003] has shown, that the wind speed process differ somewhat from being Gaussian, when evaluated in terms of the third and forth order moment. However, the scatter in these values is considerable, especially for the high wind situations with 10-minute mean wind speeds exceeding 15m/s.

5.3.2 Results

The local extreme PDF's have been evaluated for the available wind speed records, originating from the four selected sites, and subsequently compared to the theoretical prediction.

For each of the sites the available data material has been binned with respect to the mean wind speed. A bin size of 1m/s turned out to ensure a sufficient amount of observations in each mean wind speed bin and, at the same time, to allow for a suitable resolution of the mean wind speed. The binning in the mean wind speed is not required according to the theory. However, as the "degree" of Gaussian behaviour has been observed to depend on the mean wind speed, it was found appropriate. The resulting local extreme PDF's, conditioned on the mean wind speed, are presented below.

Cabauw:

The mean wind speeds range between 4m/s and 23m/s. However, the bulk of the data relates to mean wind speeds ranging from 7m/s to 19m/s, and to reduce the statistical uncertainty only records in this mean wind speed range have been used in the present analysis.

The number of local maxima identified in each of the investigated mean wind speed bins is shown in Figure (5-8). The estimated and predicted PDF's conditioned on the mean wind speed are presented in Figures (5-9) – (5-20). The predicted PDF's are based on expression (10) assuming Gaussian processes.

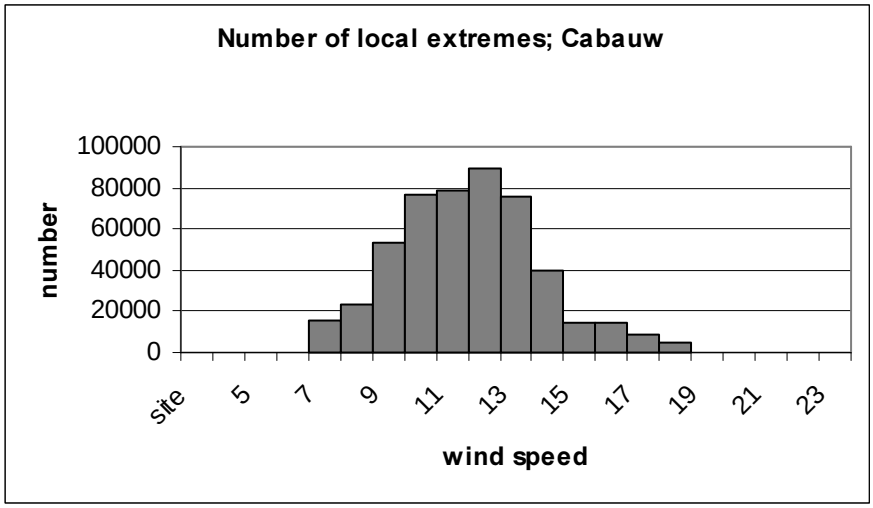

Figure 5-8 Number of identified local maxima for each of the selected mean wind speed bins.

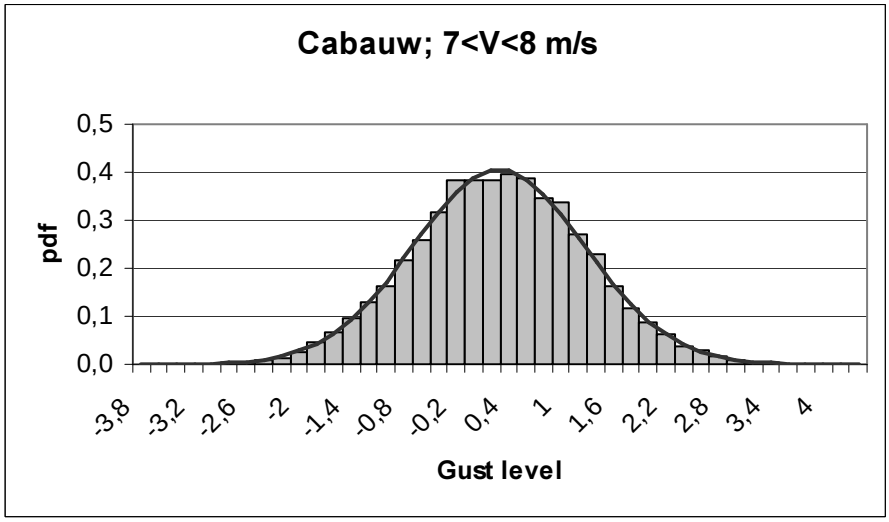

Figure 5-9 Estimated (histogram) and predicted (curve) PDF's of local normalised maxima associated with mean wind speeds in the range [7m/s;8m/s[.

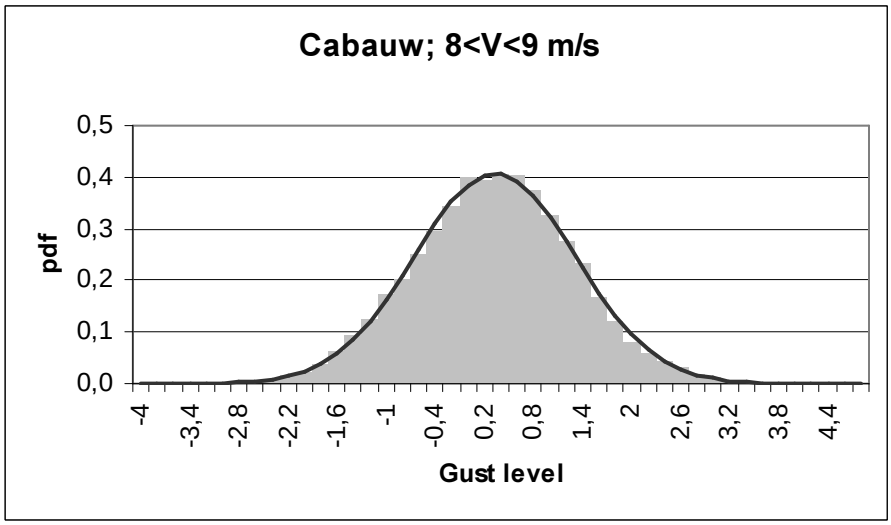

Figure 5-10 Estimated (histogram) and predicted (curve) PDF's of local normalised maxima associated with mean wind speeds in the range [8m/s;9m/s[.

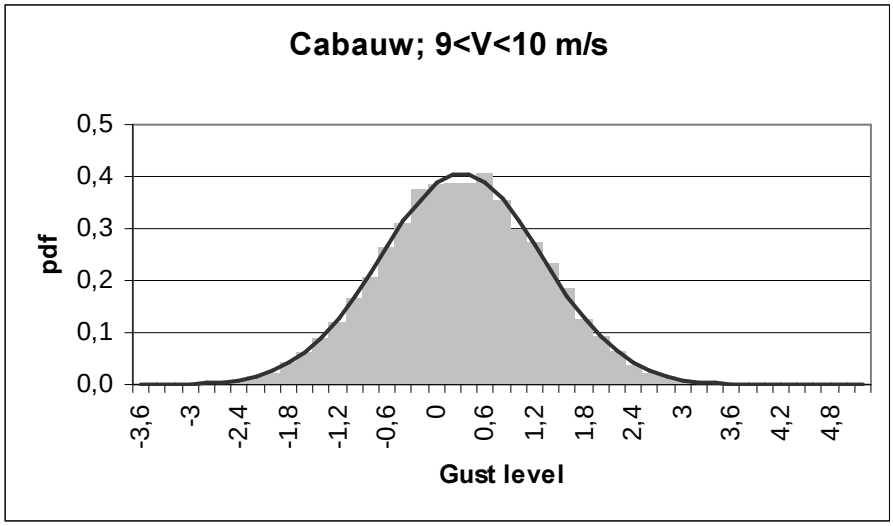

Figure 5-11 Estimated (histogram) and predicted (curve) PDF's of local normalised maxima associated with mean wind speeds in the range [9m/s;10m/s[.

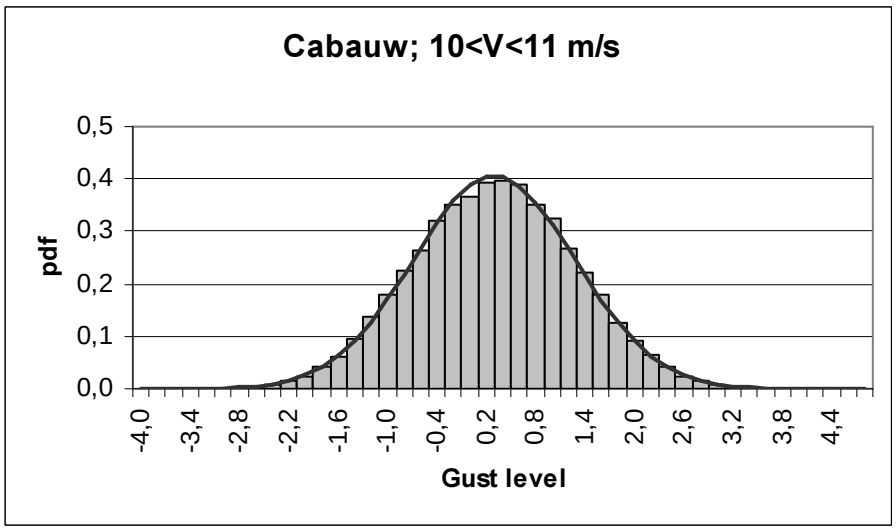

Figure 5-12 Estimated (histogram) and predicted (curve) PDF's of local normalised maxima associated with mean wind speeds in the range [10m/s;11m/s[.

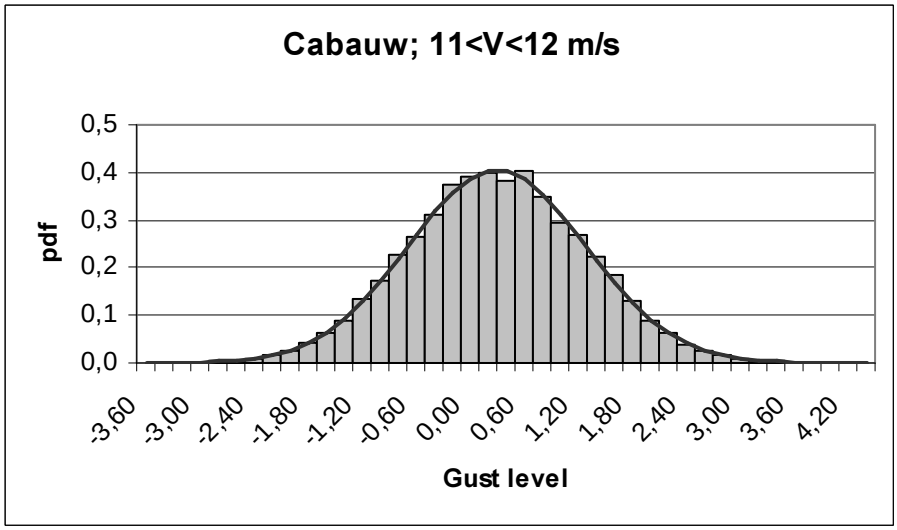

Figure 5-13 Estimated (histogram) and predicted (curve) PDF's of local normalised maxima associated with mean wind speeds in the range [11m/s;12m/s[.

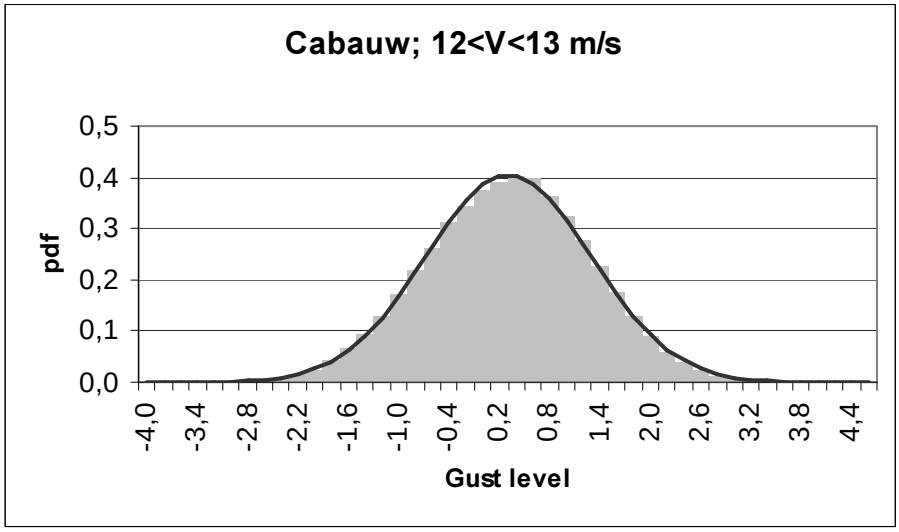

Figure 5-14 Estimated (histogram) and predicted (curve) PDF's of local normalised maxima associated with mean wind speeds in the range [12m/s;13m/s[.

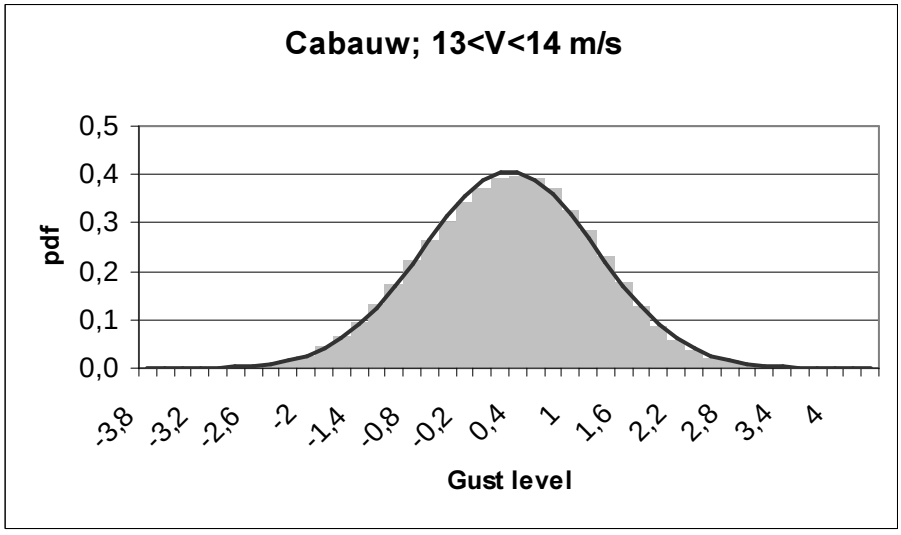

Figure 5-15 Estimated (histogram) and predicted (curve) PDF's of local normalised maxima associated with mean wind speeds in the range [13m/s;14m/s[.

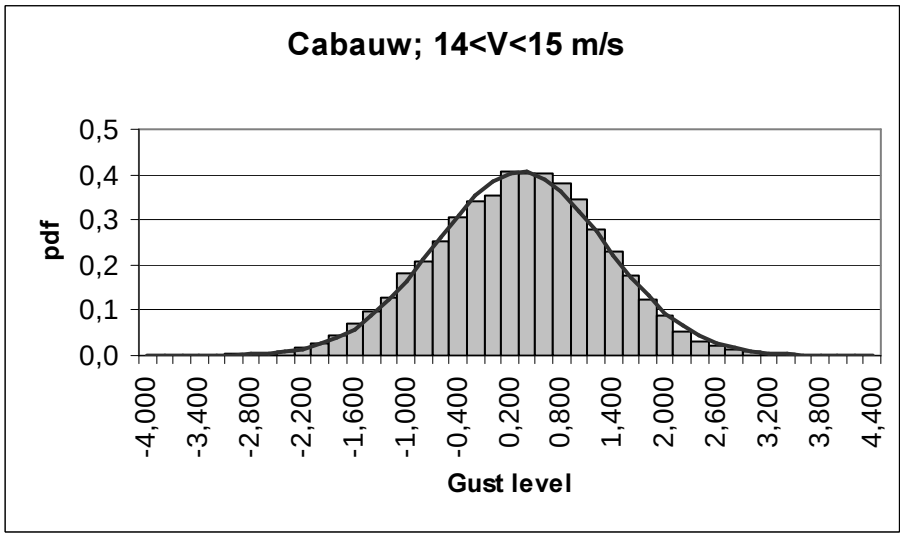

Figure 5-16 Estimated (histogram) and predicted (curve) PDF's of local normalised maxima associated with mean wind speeds in the range [14m/s;15m/s[.

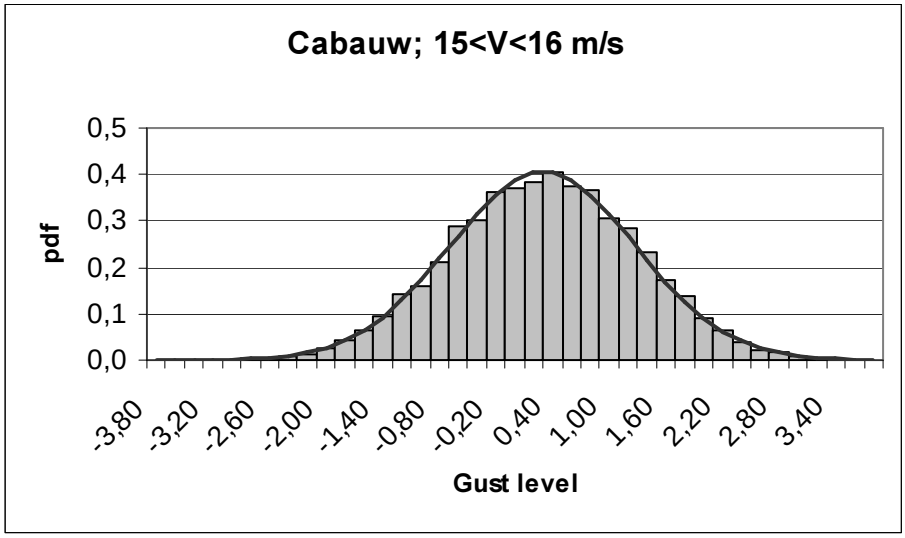

Figure 5-17 Estimated (histogram) and predicted (curve) PDF's of local normalised maxima associated with mean wind speeds in the range [15m/s;16m/s[.

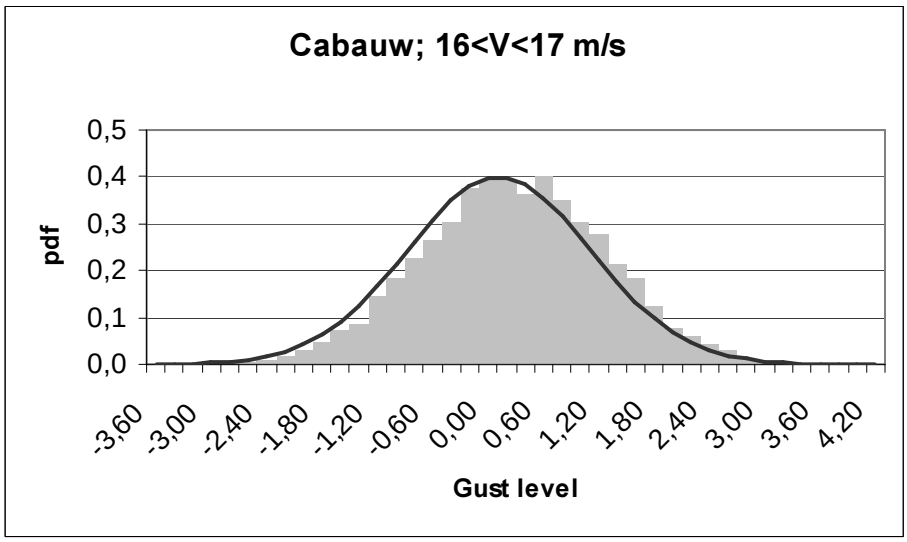

Figure 5-18 Estimated (histogram) and predicted (curve) PDF's of local normalised maxima associated with mean wind speeds in the range [16m/s;17m/s[.

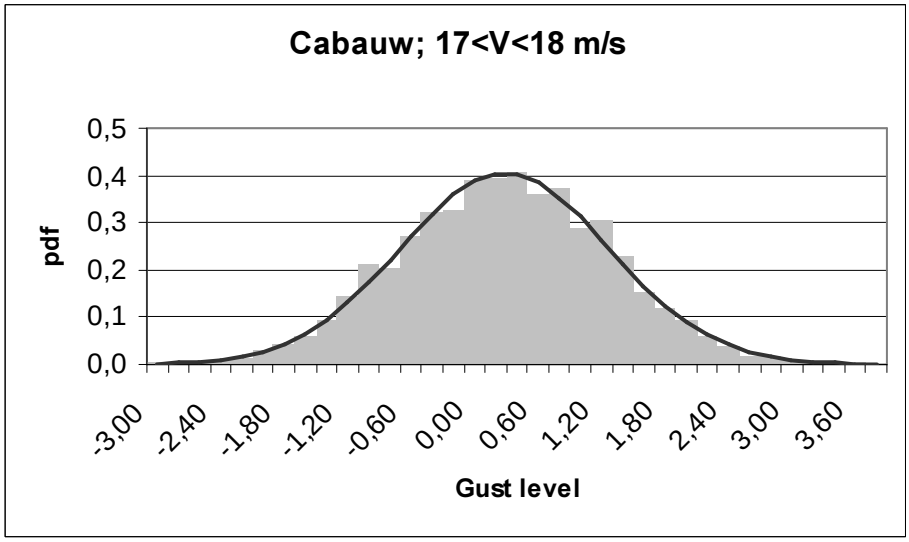

Figure 5-19 Estimated (histogram) and predicted (curve) PDF's of local normalised maxima associated with mean wind speeds in the range [17m/s;18m/s[.

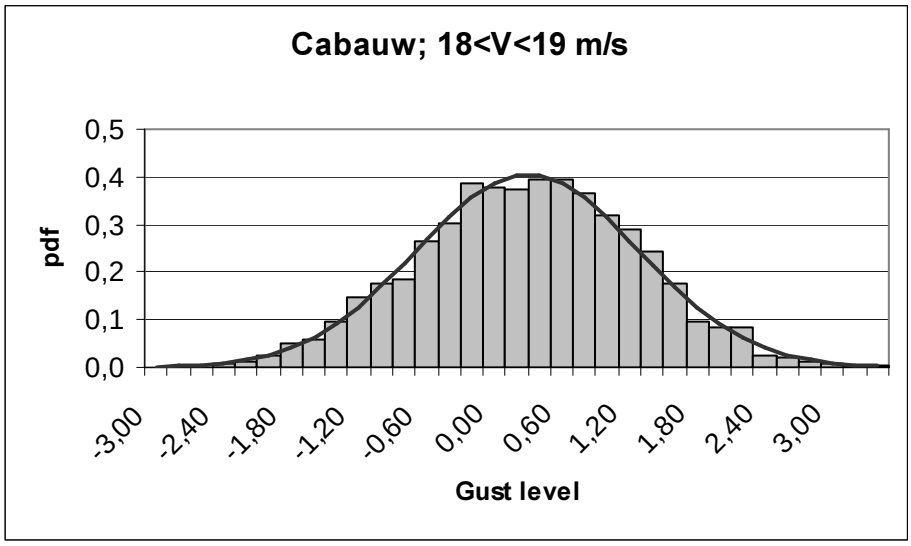

Figure 5-20 Estimated (histogram) and predicted (curve) PDF's of local normalised maxima associated with mean wind speeds in the range [18m/s;19m/s[.

As seen there is an impressive agreement between the estimated and the predicted PDF's for all the investigated mean wind bins. This is in good agreement with the analysis in [Larsen, 2003-] indicating a Gaussian behaviour of the investigated wind speed time series, as the Gaussian behaviour is the basic assumption for the derived theoretical model.

The bandwidth parameter is almost independent of the mean wind speed (equal to 0.97 for 10 of the 12 investigated mean wind speed bins, and equal to 0.99 and 0.96, respectively, for the remaining two mean wind speed bins). The high values (close to one) indicate, as expected, that the measured turbulence is indeed broad-banded. The resulting local extreme PDF's are consequently seen to be close to Gaussian.

Vindeby (on-shore):

The mean wind speeds range between 5m/s and 21m/s. However, the bulk of the data relates to mean wind speeds ranging from 5m/s to 19m/s, and in order to reduce the statistical uncertainty only records within this mean wind speed range have been utilised in the present analysis. The total number of local maxima, identified in each of the investigated mean wind speed bins, is presented in Figure (5-21).

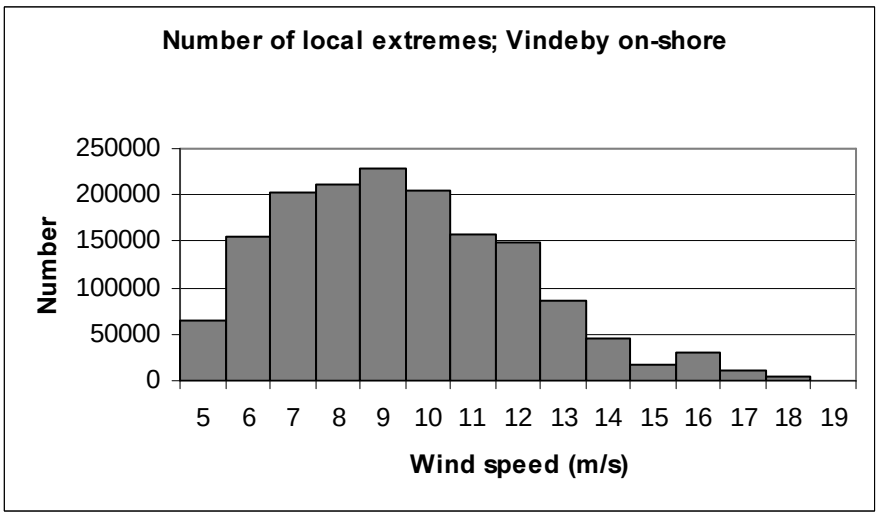

Figure 5-21 Number of identified local maxima for each individual mean wind speed bin.

The estimated and predicted PDF's conditioned on the mean wind speed are presented in Figures (5-22) – (5-35). All the predicted PDF's are based on expression (10) assuming Gaussian wind speed processes.

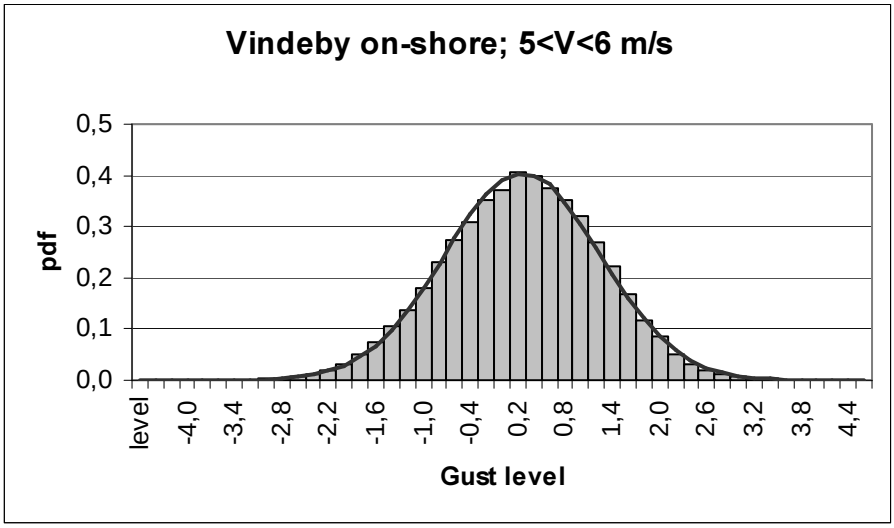

Figure 5-22 Estimated (histogram) and predicted (curve) PDF's of local normalised maxima associated with mean wind speeds in the range [5m/s;6m/s[.

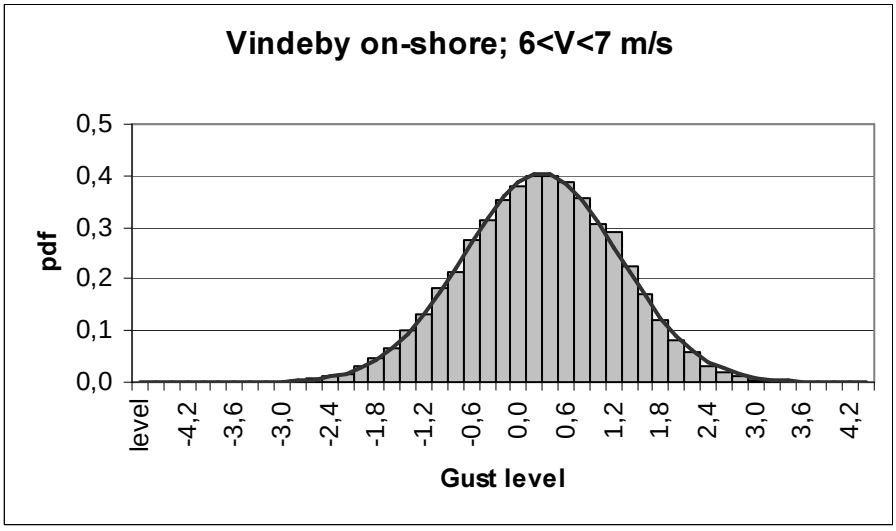

Figure 5-23 Estimated (histogram) and predicted (curve) PDF's of local normalised maxima associated with mean wind speeds in the range [6m/s;7m/s[.

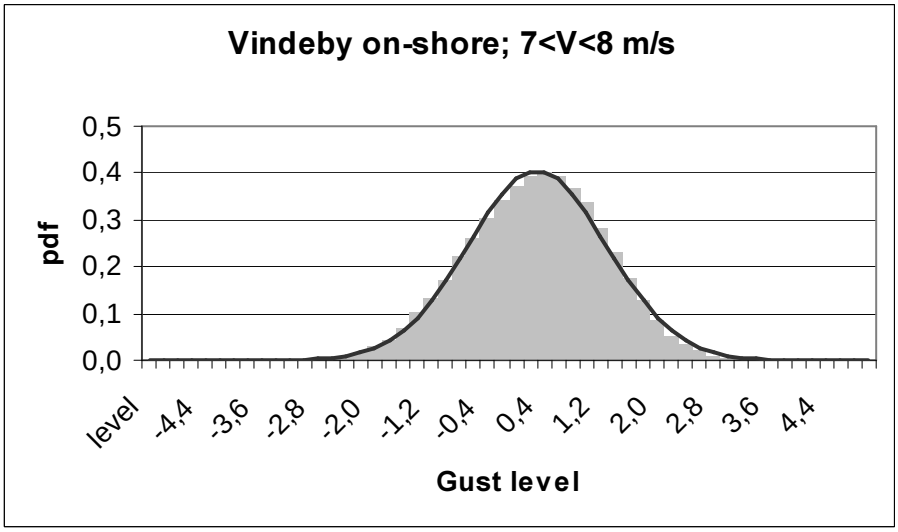

Figure 5-24 Estimated (histogram) and predicted (curve) PDF's of local normalised maxima associated with mean wind speeds in the range [7m/s;8m/s[.

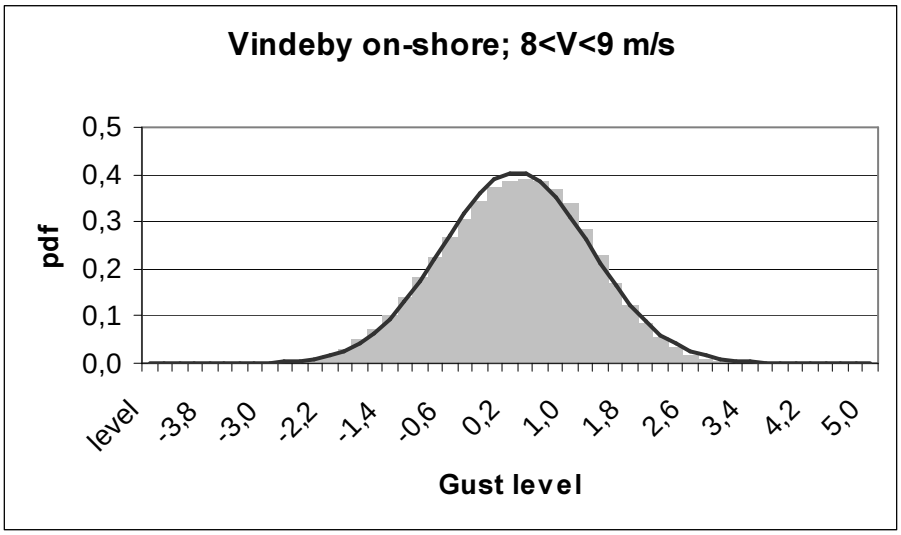

Figure 5-25 Estimated (histogram) and predicted (curve) PDF's of local normalised maxima associated with mean wind speeds in the range [8m/s;9m/s[.

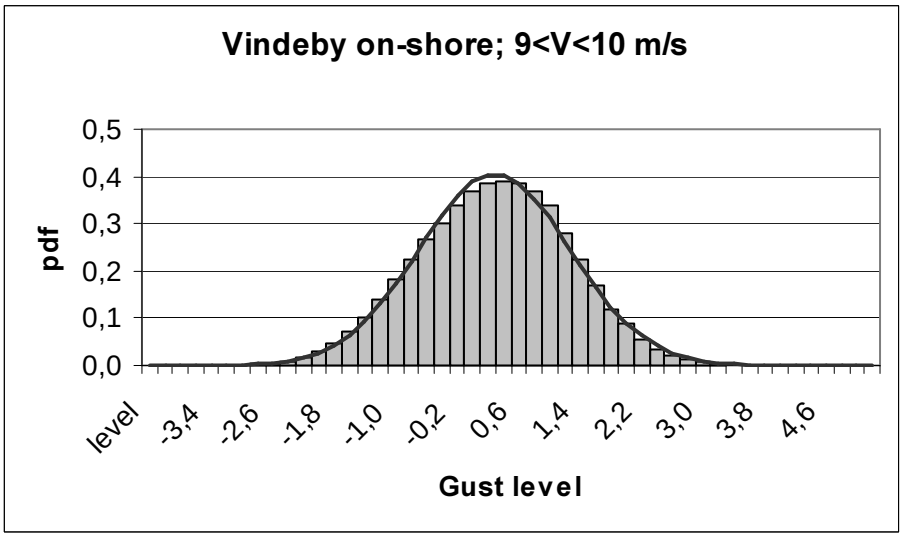

Figure 5-26 Estimated (histogram) and predicted (curve) PDF's of local normalised maxima associated with mean wind speeds in the range [9m/s;10m/s[.

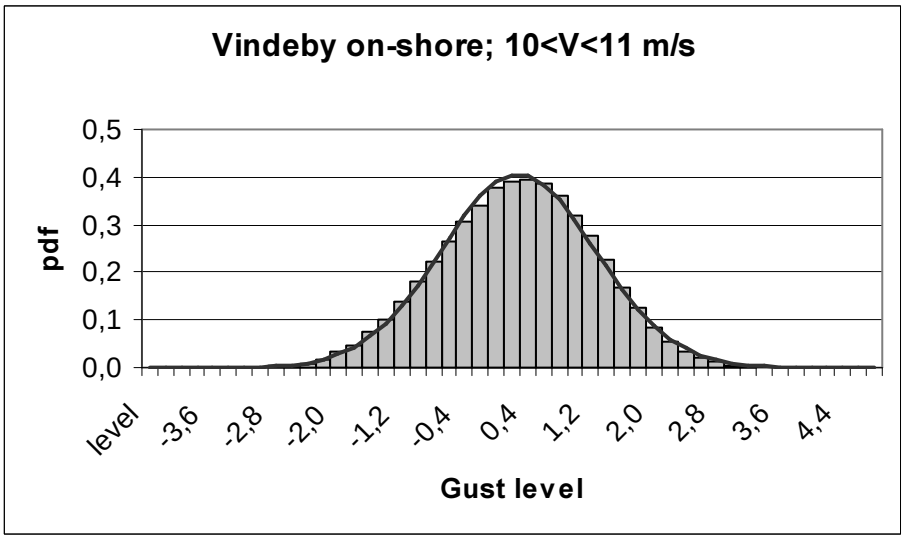

Figure 5-27 Estimated (histogram) and predicted (curve) PDF's of local normalised maxima associated with mean wind speeds in the range [10m/s;11m/s[.

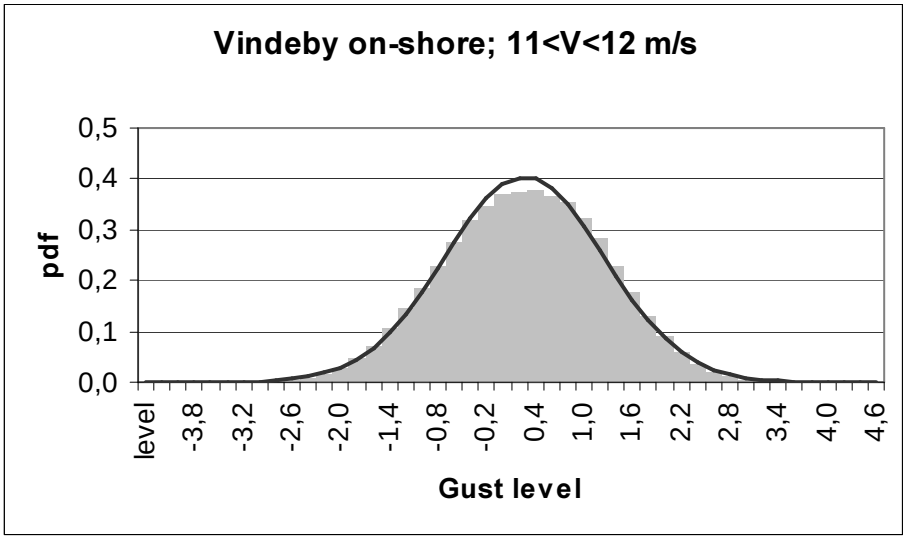

Figure 5-28 Estimated (histogram) and predicted (curve) PDF's of local normalised maxima associated with mean wind speeds in the range [11m/s;12m/s[.

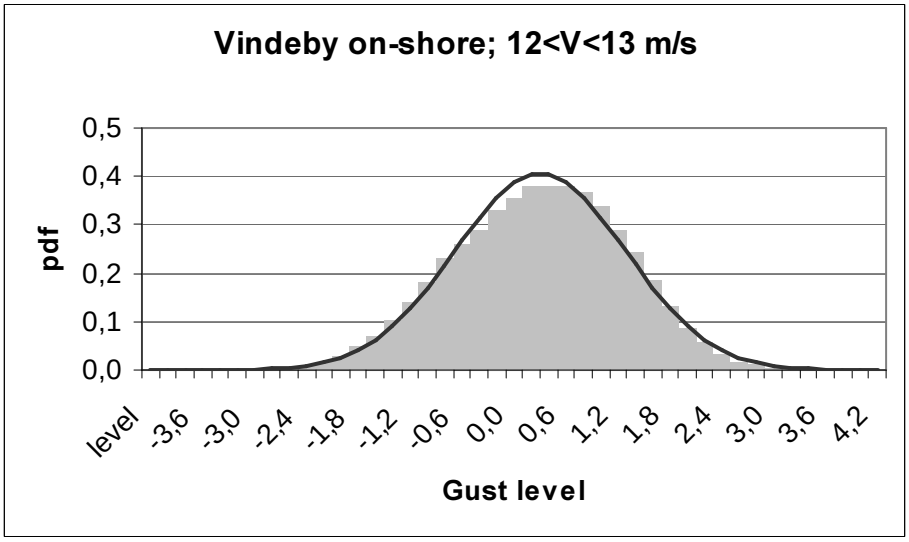

Figure 5-29 Estimated (histogram) and predicted (curve) PDF's of local normalised maxima associated with mean wind speeds in the range [12m/s;13m/s[.

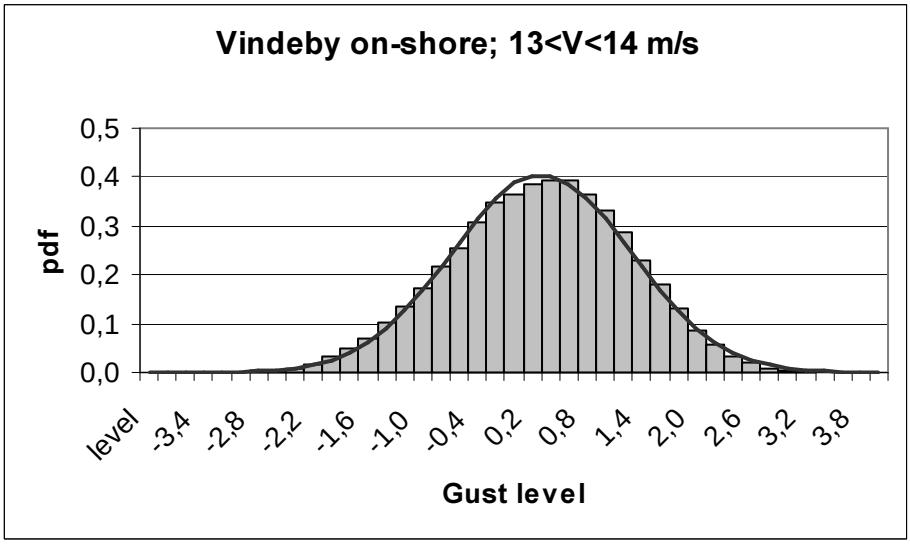

Figure 5-30 Estimated (histogram) and predicted (curve) PDF's of local normalised maxima associated with mean wind speeds in the range [13m/s;14m/s[.

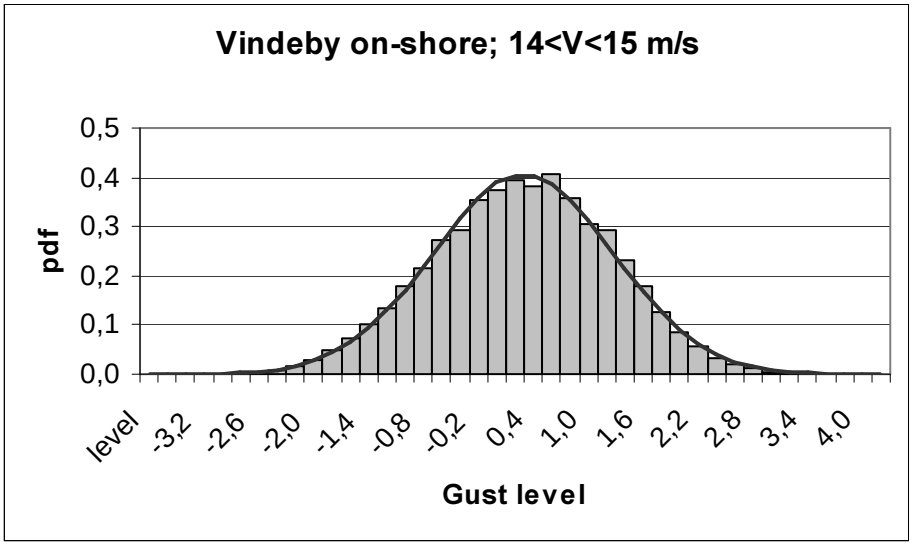

Figure 5-31 Estimated (histogram) and predicted (curve) PDF's of local normalised maxima associated with mean wind speeds in the range [14m/s;15m/s[.

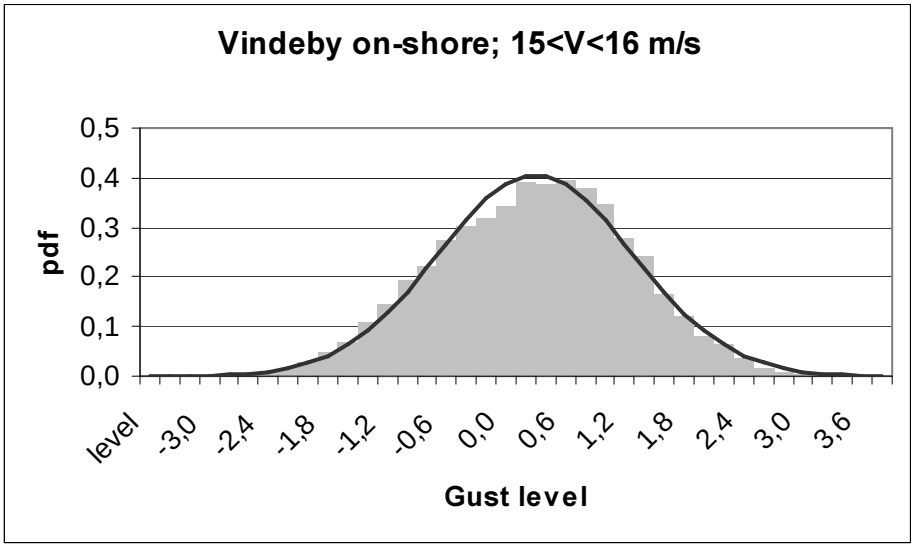

Figure 5-32 Estimated (histogram) and predicted (curve) PDF's of local normalised maxima associated with mean wind speeds in the range [15m/s;16m/s[.

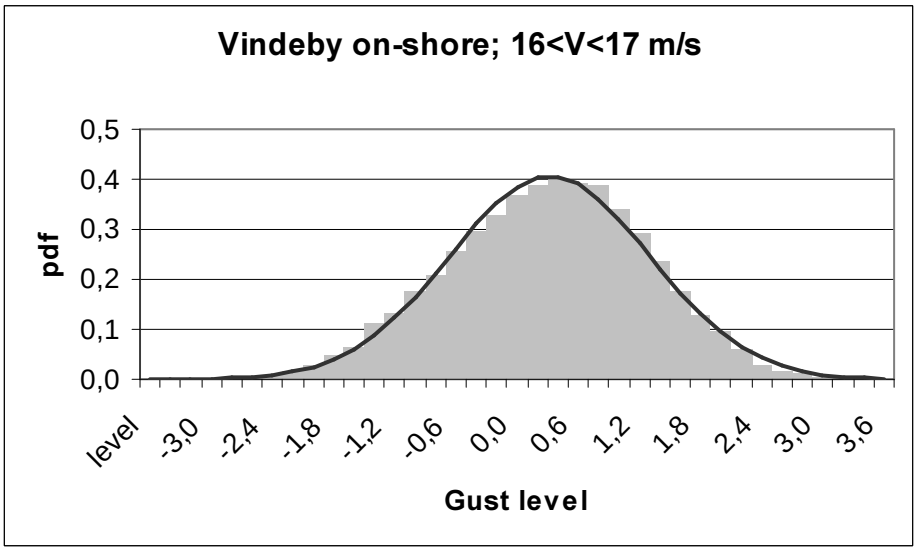

Figure 5-33 Estimated (histogram) and predicted (curve) PDF's of local normalised maxima associated with mean wind speeds in the range [16m/s;17m/s[.

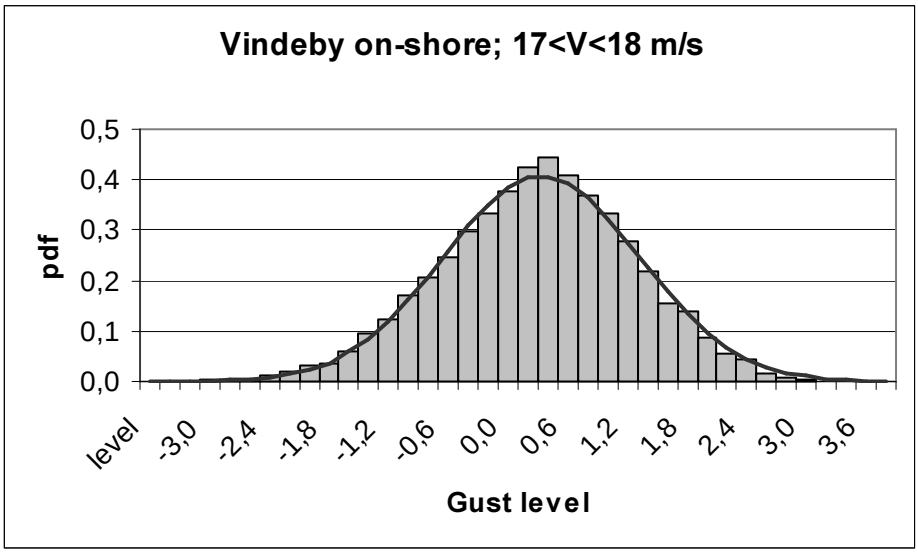

Figure 5-34 Estimated (histogram) and predicted (curve) PDF's of local normalised maxima associated with mean wind speeds in the range [17m/s;18m/s[.

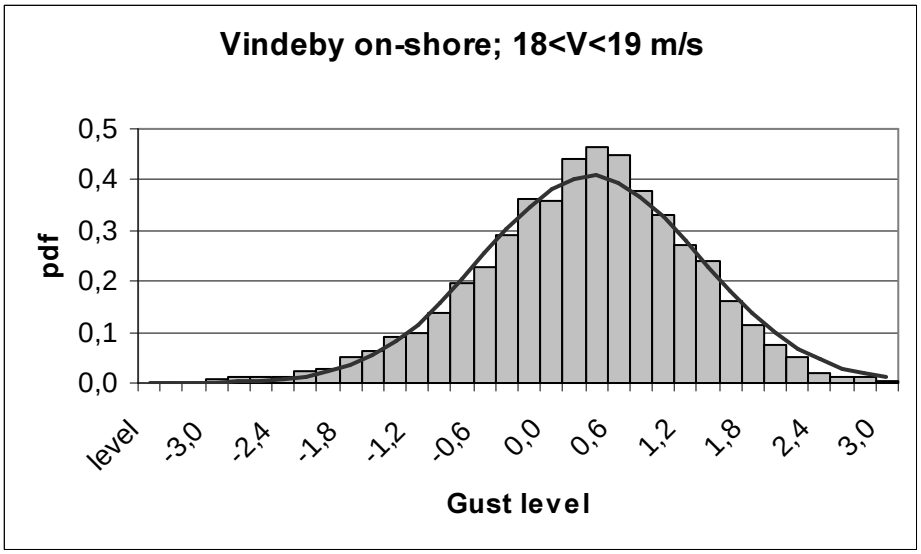

Figure 5-35 Estimated (histogram) and predicted (curve) PDF's of local normalised maxima associated with mean wind speeds in the range [18m/s;19m/s[.

The predicted PDF's for the local extremes are seen to fit the estimated PDF's very well at this coastal site. The agreement between predictions and measurements is very satisfactory for all the investigated mean wind speed bins, and is considered to be due to a close to Gaussian behaviour of the bulk of the investigated wind speed time series.

The bandwidth parameter is almost independent of the mean wind speed (equal to 0.97 for 10 of the 14 investigated mean wind speed bins, equal to 0.98 for 2 mean wind speed bins and equal to 0.96 for the remaining 2 mean wind speed bins). The high values (close to one) indicate, as expected, that the measured turbulence is indeed broad-banded. In accordance herewith, the resulting local extreme PDF's are seen to be close to Gaussian.

Vindeby (off-shore):

The mean wind speeds range between 5m/s and 25m/s. However, the bulk of the data relates to mean wind speeds ranging from 7m/s to 19m/s, and in order to reduce the statistical uncertainty only records within this mean wind speed range have been utilised in the present analysis.

The number of local maxima, identified in each of the investigated mean wind speed bins, is given in Figure (5-36).

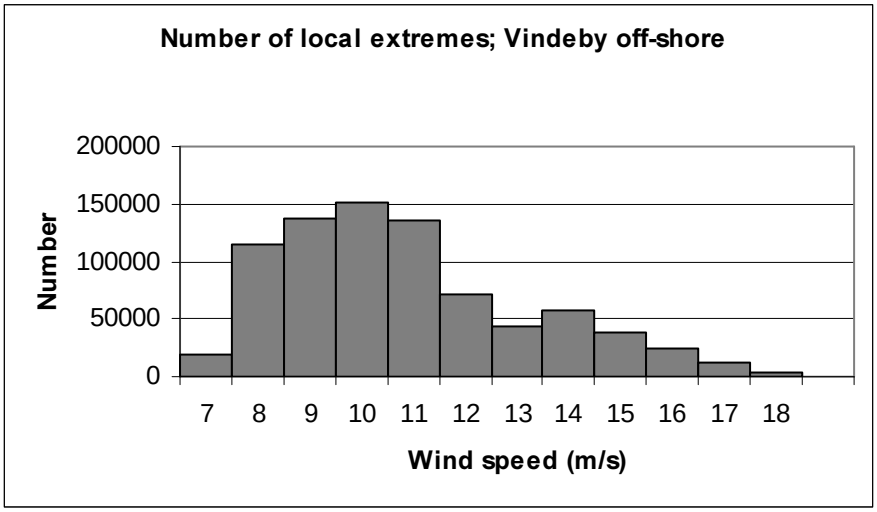

Figure 5-36 Number of identified local maxima for each individual mean wind speed bin.

The estimated and predicted PDF's, conditioned on the mean wind speed, are presented in the Figures (5-37) – (5-48). As for the two preceding site investigations, all the predicted PDF's are based on expression (10) assuming Gaussian or close to Gaussian wind speed processes.

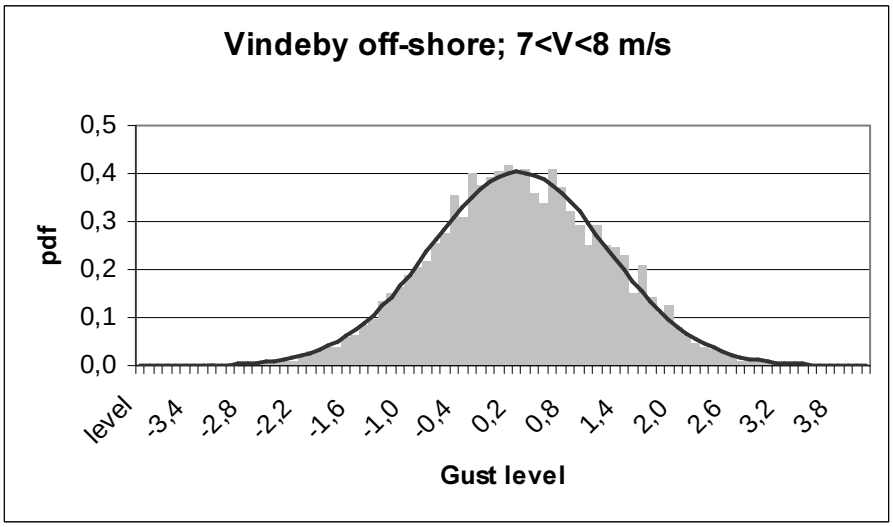

Figure 5-37 Estimated (histogram) and predicted (curve) PDF's of local normalised maxima associated with mean wind speeds in the range [7m/s;8m/s[.

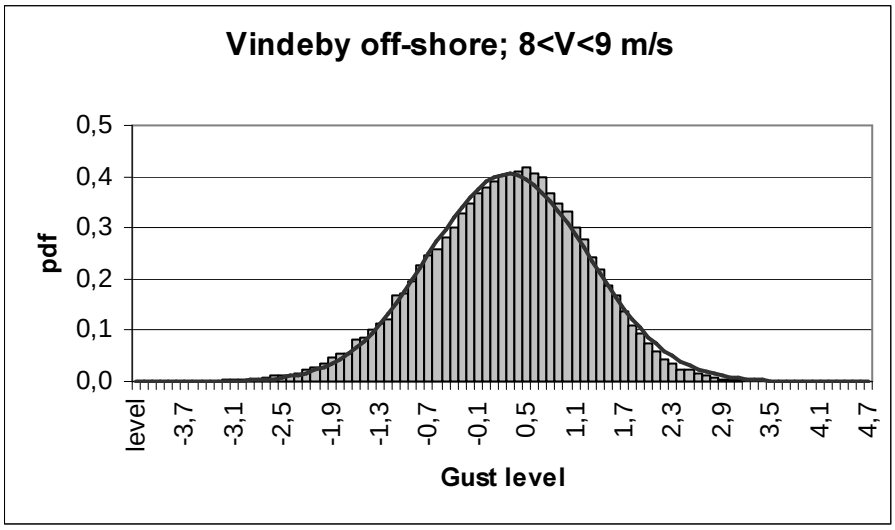

Figure 5-38 Estimated (histogram) and predicted (curve) PDF's of local normalised maxima associated with mean wind speeds in the range [8m/s;9m/s[.

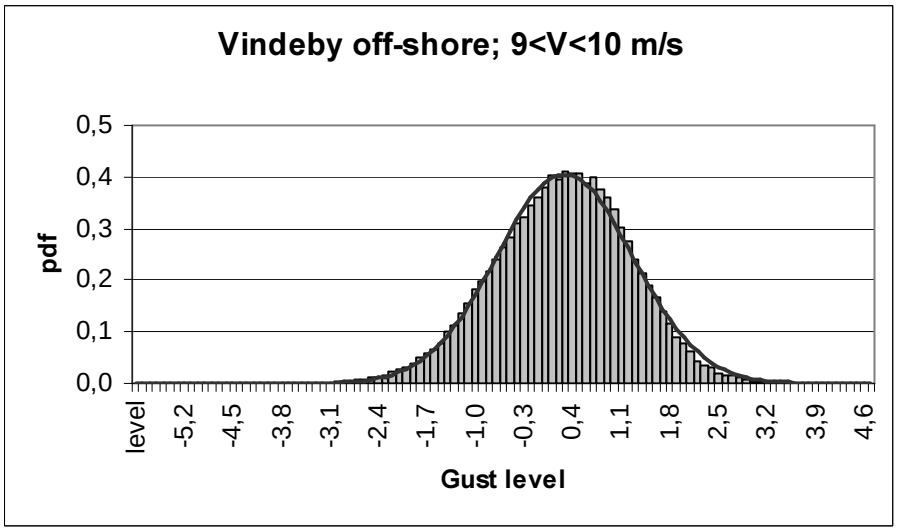

Figure 5-39 Estimated (histogram) and predicted (curve) PDF's of local normalised maxima associated with mean wind speeds in the range [9m/s;10m/s[.

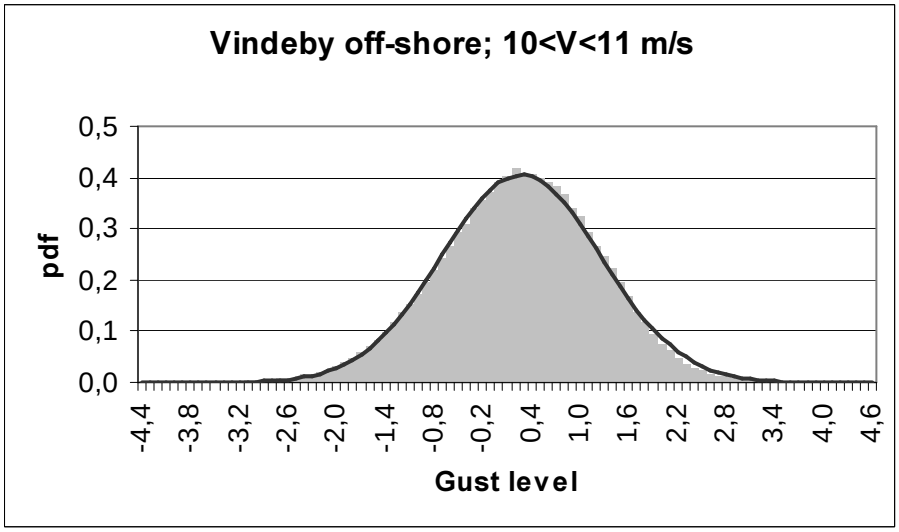

Figure 5-40 Estimated (histogram) and predicted (curve) PDF's of local normalised maxima associated with mean wind speeds in the range [10m/s;11m/s[.

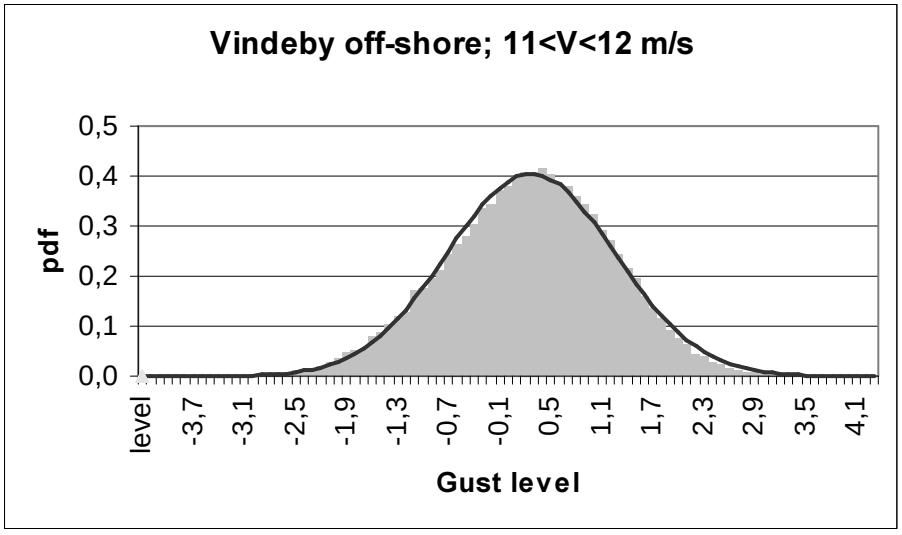

Figure 5-41 Estimated (histogram) and predicted (curve) PDF's of local normalised maxima associated with mean wind speeds in the range [11m/s;12m/s[.

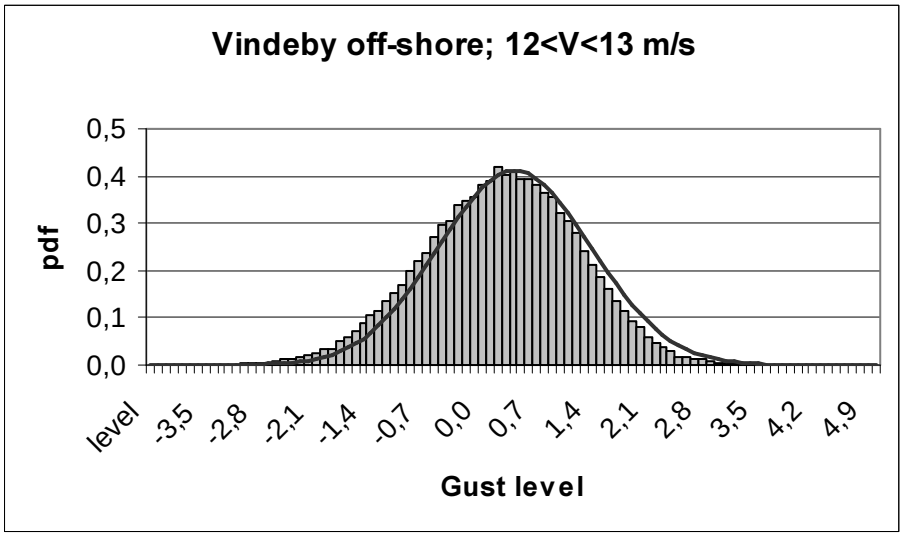

Figure 5-42 Estimated (histogram) and predicted (curve) PDF's of local normalised maxima associated with mean wind speeds in the range [12m/s;13m/s[.

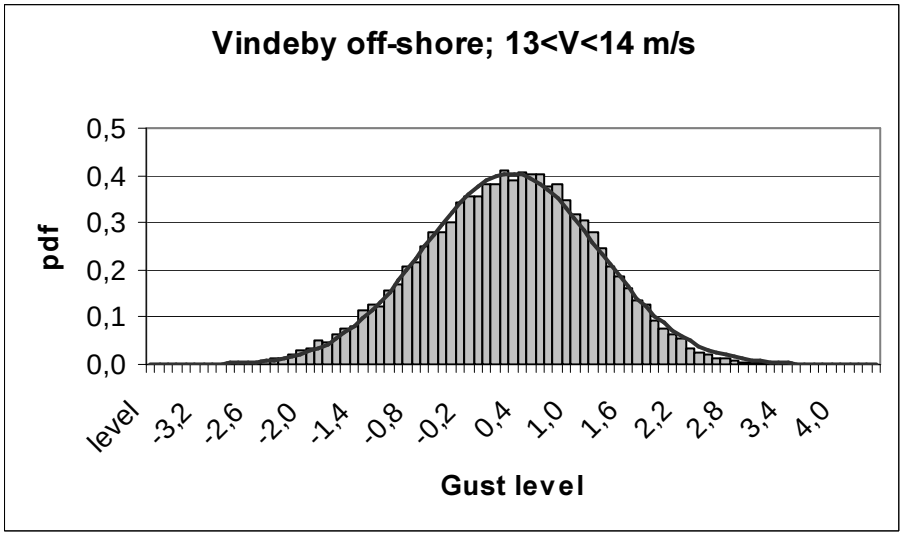

Figure 5-43 Estimated (histogram) and predicted (curve) PDF's of local normalised maxima associated with mean wind speeds in the range [13m/s;14m/s[.

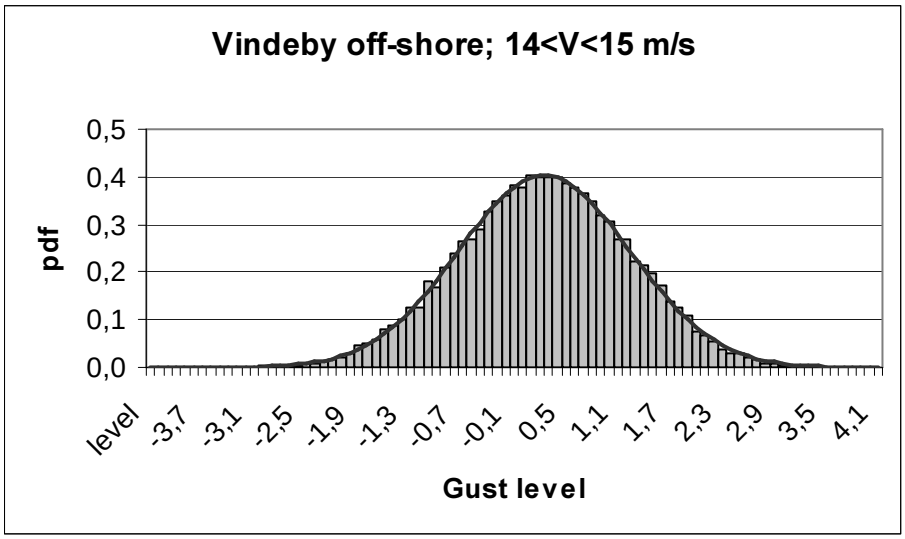

Figure 5-44 Estimated (histogram) and predicted (curve) PDF's of local normalised maxima associated with mean wind speeds in the range [14m/s;15m/s[.

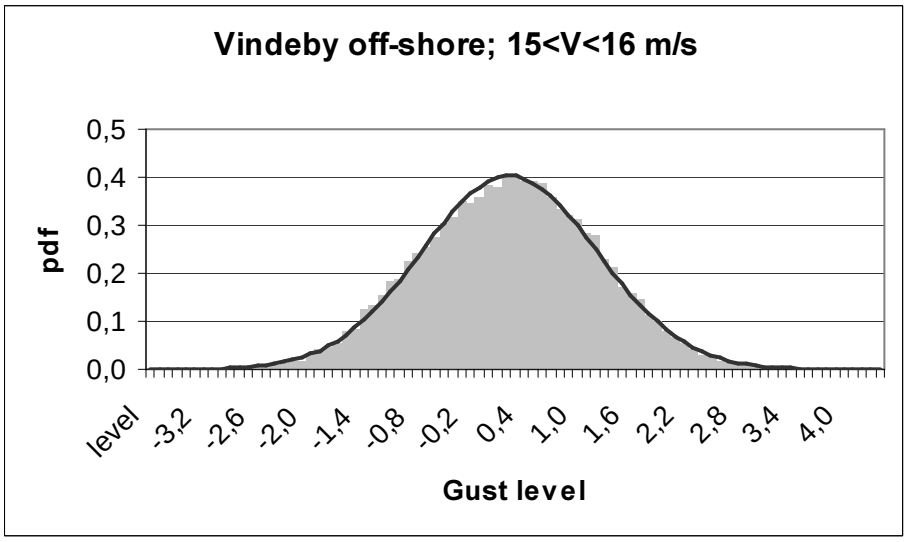

Figure 5-45 Estimated (histogram) and predicted (curve) PDF's of local normalised maxima associated with mean wind speeds in the range [15m/s;16m/s[.

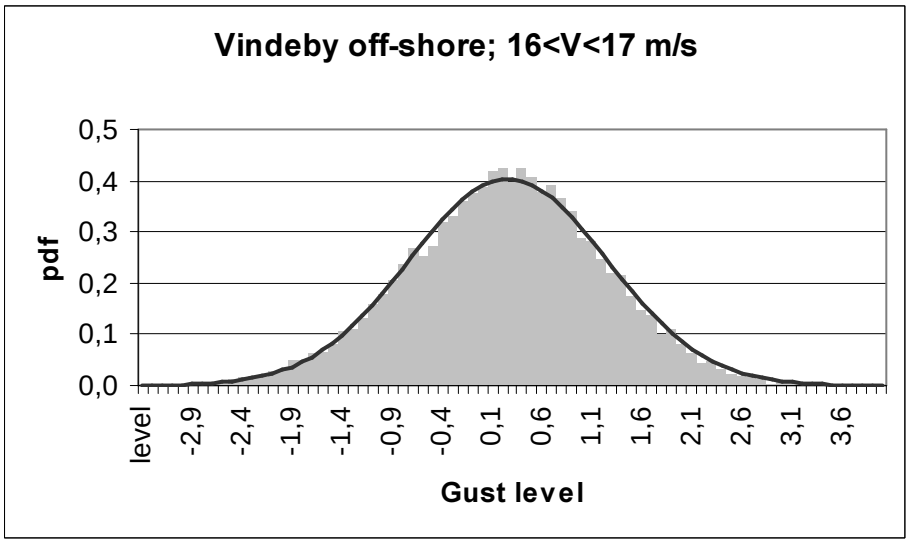

Figure 5-46 Estimated (histogram) and predicted (curve) PDF's of local normalised maxima associated with mean wind speeds in the range [16m/s;17m/s[.

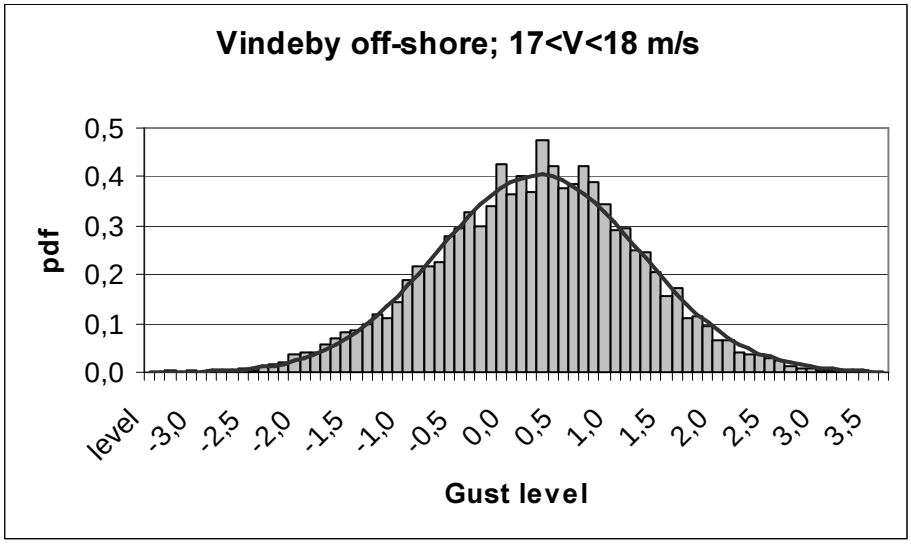

Figure 5-47 Estimated (histogram) and predicted (curve) PDF's of local normalised maxima associated with mean wind speeds in the range [17m/s;18m/s[.

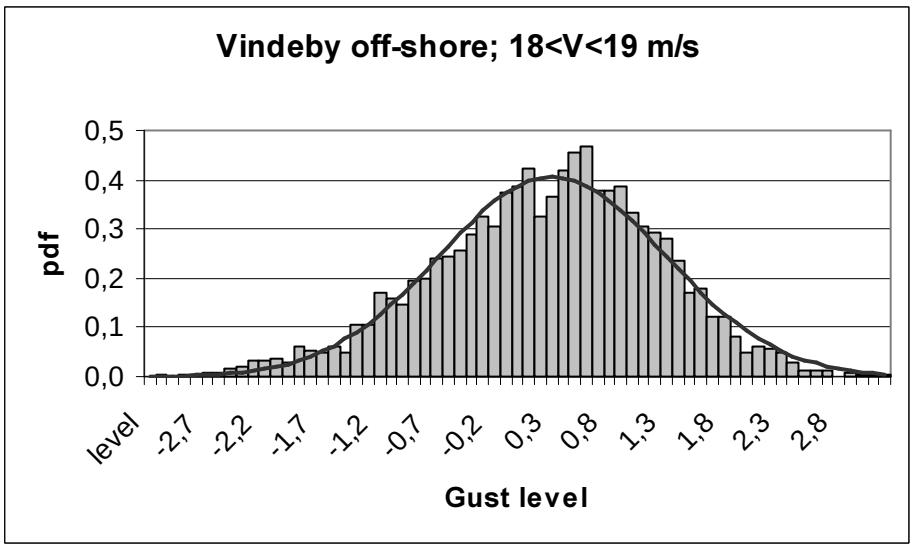

Figure 5-48 Estimated (histogram) and predicted (curve) PDF's of local normalised maxima associated with mean wind speeds in the range [18m/s;19m/s[.

The statistics of the Vindeby off-shore data is qualitative analogue to the statistics of the Vindeby on-shore site and of the Cabauw site in the sense that all the predicted PDF's for the local extremes are seen to fit well with the estimated PDF's. Again, this considered to be due to a close to Gaussian behaviour of the bulk of the investigated wind speed time series.

Also for these data, the bandwidth parameter is almost independent of the mean wind speed (equal to 0.98 for 9 of the 12 investigated mean wind speed bins, equal to 0.97 for 2 mean wind speed bins and equal to 0.94 for one mean wind speed wind). The high values (close to one) indicate, as expected, that the measured turbulence is indeed broad-banded, and, as a consequence, the resulting local extreme PDF's are seen to be close to Gaussian distributed.

Oak Creek:

The Oak Creek site differs considerably from the previously investigated sites as the terrain is very complex with a high annual mean wind speed. Moreover, the statistics of the measured wind speeds differ somewhat from a Gaussian behaviour for some of the analysed mean wind speed bins.

The mean wind speeds range between 5m/s and 28m/s. However, the bulk of the data relates to mean wind speeds ranging from 5m/s to 25m/s, and in order to reduce the statistical uncertainty only records within this mean wind speed range have been utilised in the present analysis.

The number of local maxima, identified in each of the investigated mean wind speed bins, is shown in Figure (5-49).

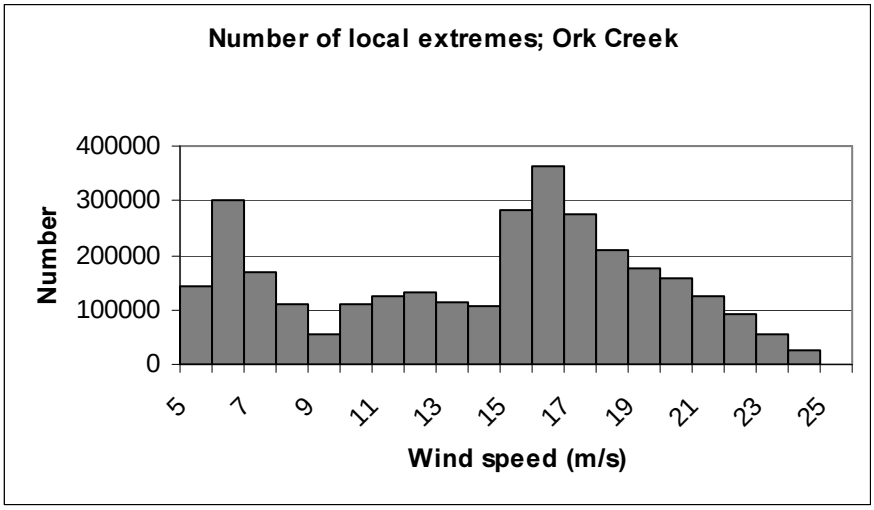

Figure 5-49 Number of identified local maxima for each individual mean wind speed bin.

The "degree" of Gaussian behaviour of the investigated time series is illustrated in Figures (5-50), (5-51). Figure (5-50) shows, for each of the selected mean wind speed bins, the mean skewness of all wind speed time series associated with the particular bin. Analogues, Figure (5-51) shows the mean kurtosis of wind speed time series associated with a particular mean wind speed bin.

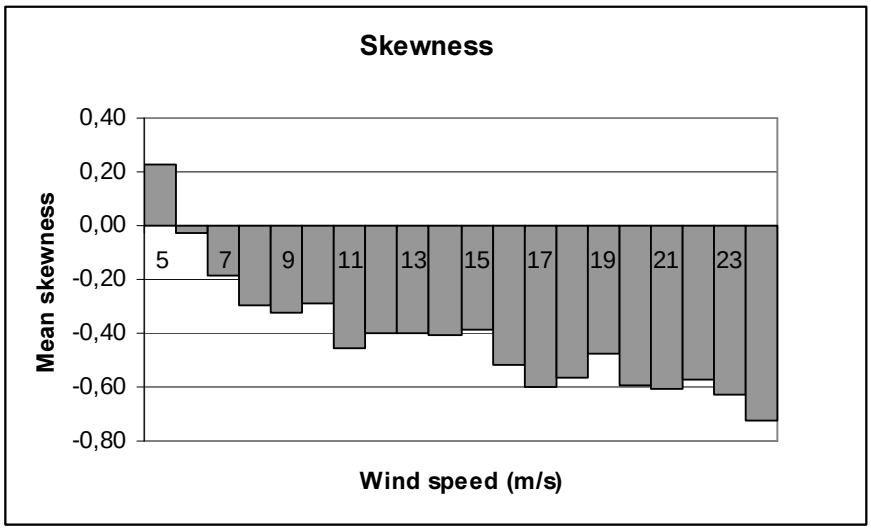

Figure 5-50 Mean skewness as function of mean wind speed bin.

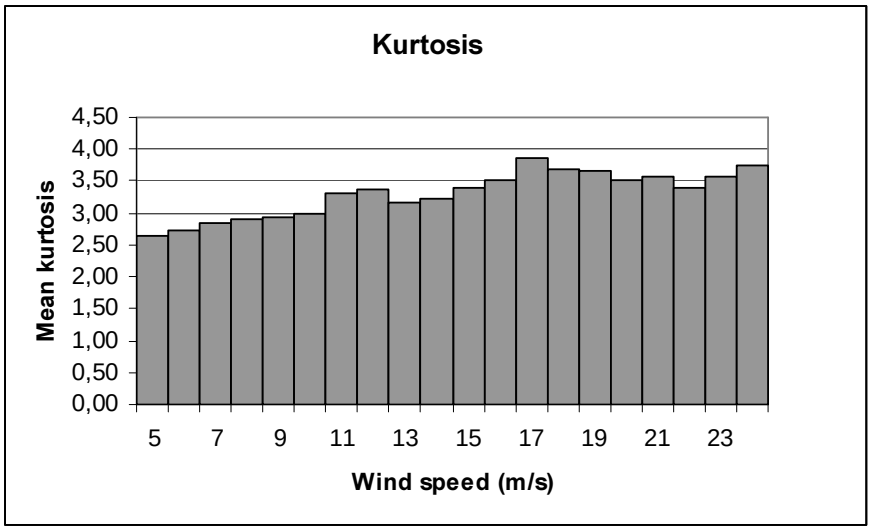

Figure 5-51 Mean kurtosis as function of mean wind speed bin.

Figures (5-50-51) indicates a tendency of increasing deviation from a Gaussian behaviour with increasing mean wind speed. It is difficult a priori to judge how robust a prediction based on expression (10), assuming Gaussian behaviour of the underlying stochastic process, is to violations of this assumption. In the present study, a simple operational, but rather arbitrary, choice have been to apply a prediction based on expression (10) for mean values of the numerical value of the skewness less than 0.4. The choice is based on a visual inspection of the degree of agreement between a prediction based on (10) and the respective estimated distribution based on the observed local maxima. For mean wind speed bins where the mean (numerical value of the) skewness exceeds 0.4, the theoretical prediction is based on expression (20). However, to illustrate the difference also predictions based on expression (10) are given for these wind speed bins.

The estimated and predicted PDF's, conditioned on the mean wind speed, are presented in the Figures (5-52) – (5-86). Where the predicted PDF's are based on expression (10) the estimated distributions are illustrated in terms of histograms – when the predicted PDF's are based on expression (20) the estimated distributions are illustrated in terms of dots.

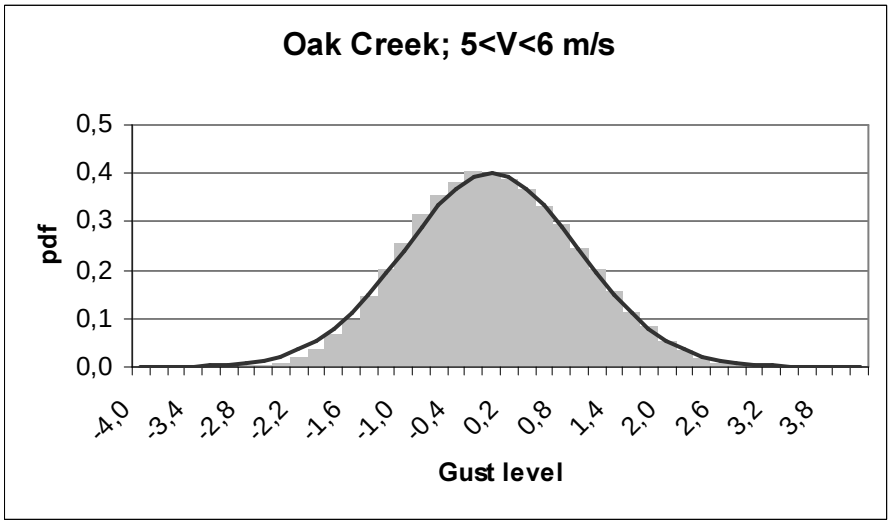

Figure 5-52 Estimated (histogram) and predicted (curve) PDF's of local normalised maxima. The prediction is based on expression (10).

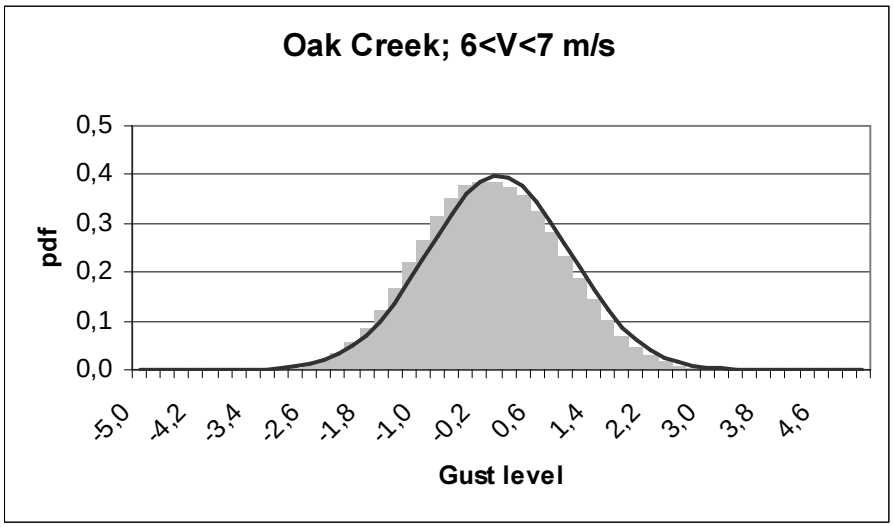

Figure 5-53 Estimated (histogram) and predicted (curve) PDF's of local normalised maxima. The prediction is based on expression (10).

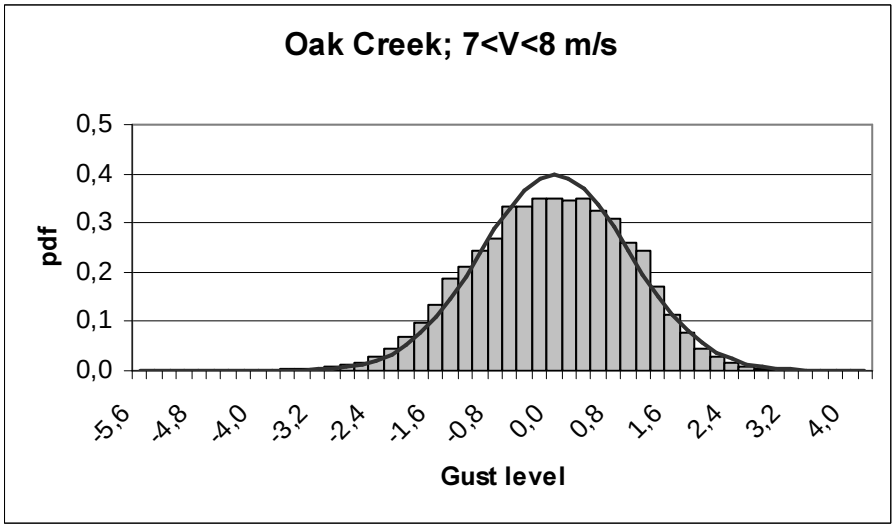

Figure 5-54 Estimated (histogram) and predicted (curve) PDF's of local normalised maxima. The prediction is based on expression (10).

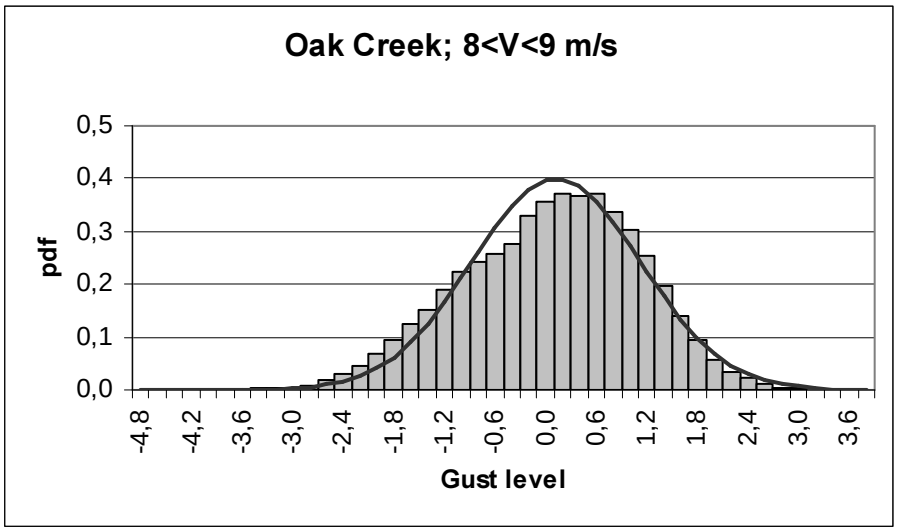

Figure 5-55 Estimated (histogram) and predicted (curve) PDF's of local normalised maxima. The prediction is based on expression (10).

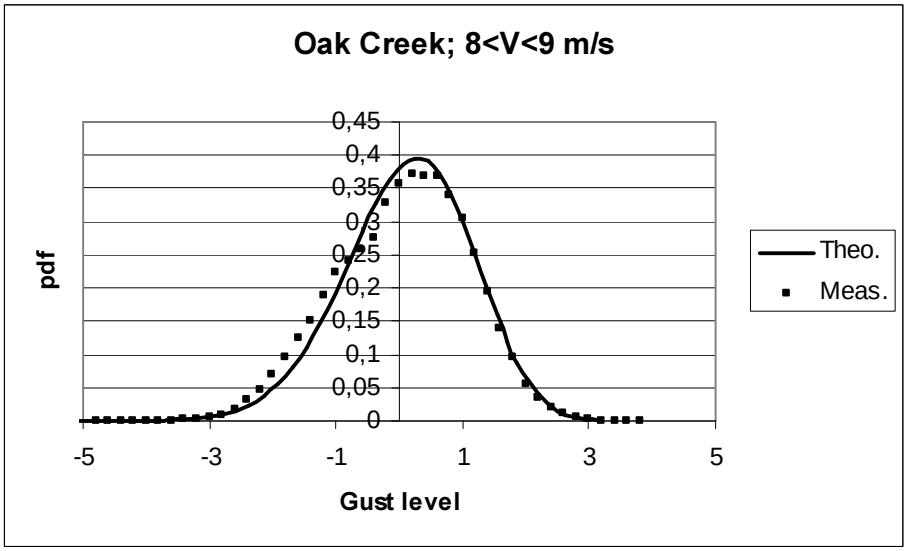

Figure 5-56 Estimated (squares) and predicted (curve) PDF's of local normalised maxima. The prediction is based on expression (20).

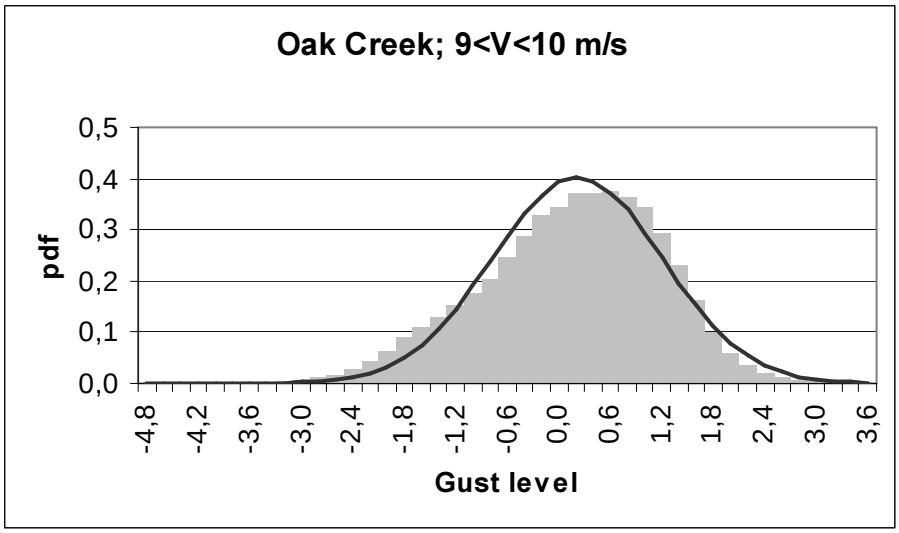

Figure 5-57 Estimated (histogram) and predicted (curve) PDF's of local normalised maxima. The prediction is based on expression (10).

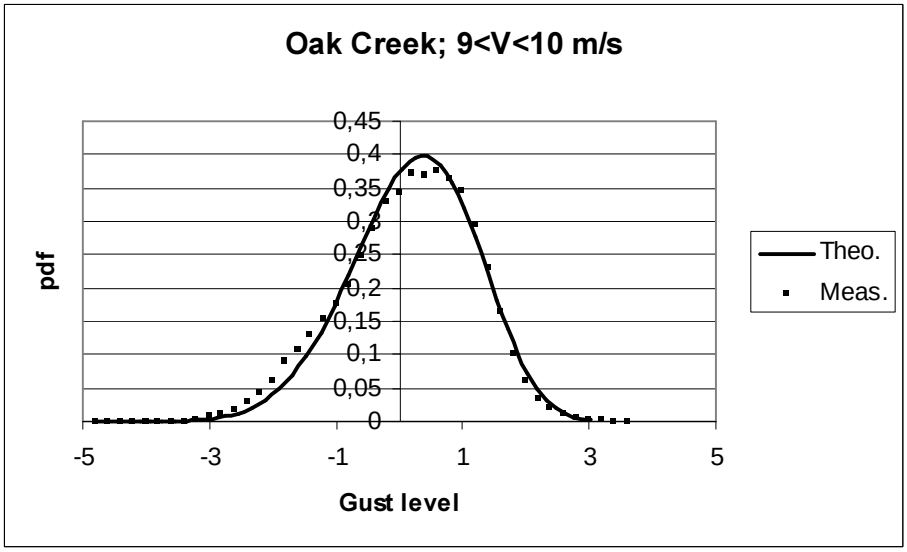

Figure 5-58 Estimated (squares) and predicted (curve) PDF's of local normalised maxima. The prediction is based on expression (20).

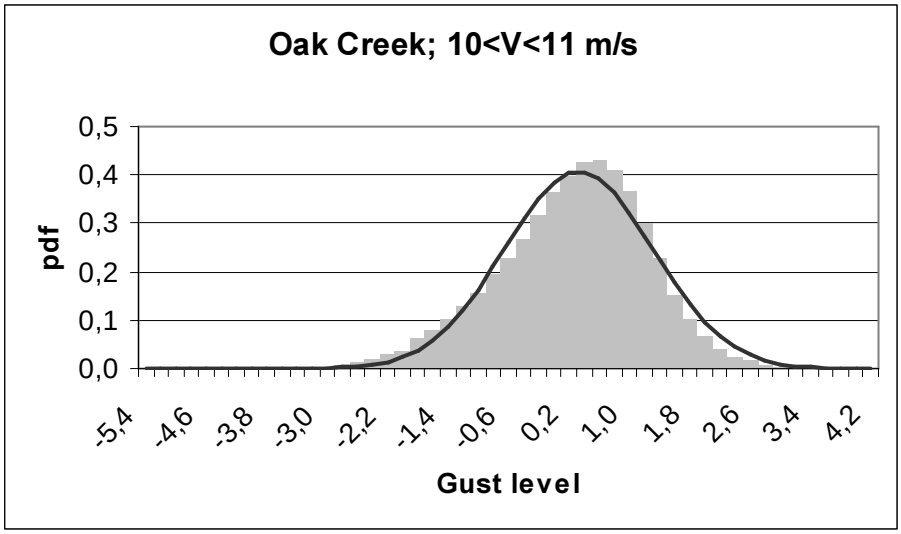

Figure 5-59 Estimated (histogram) and predicted (curve) PDF's of local normalised maxima. The prediction is based on expression (10).

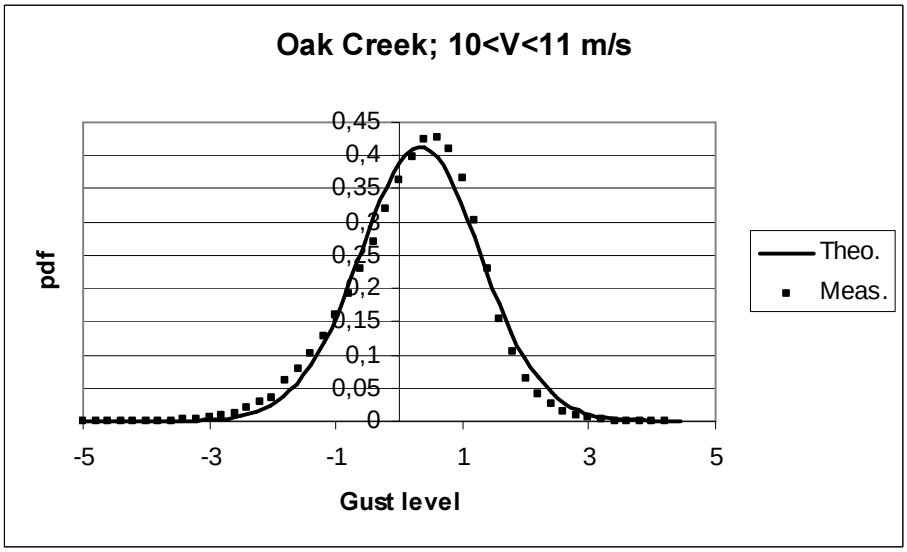

Figure 5-60 Estimated (squares) and predicted (curve) PDF's of local normalised maxima. The prediction is based on expression (20).

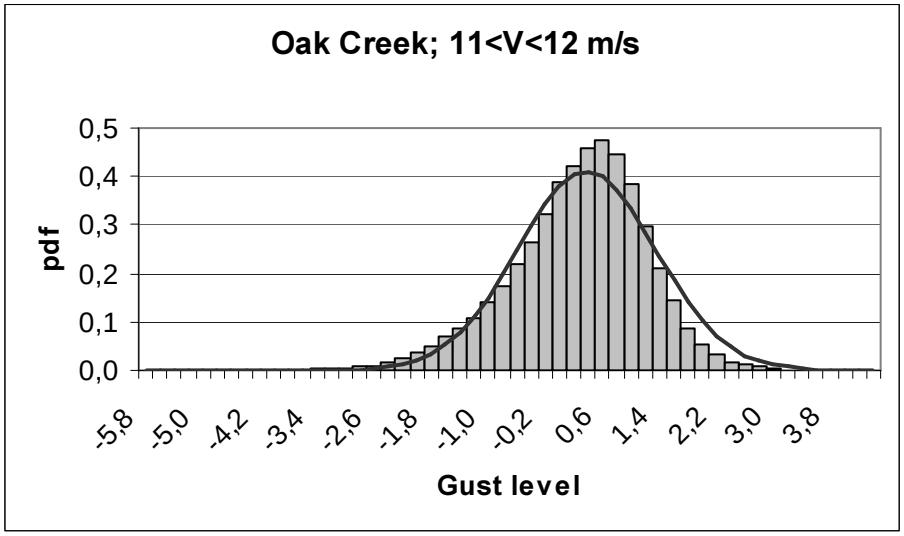

Figure 5-61 Estimated (histogram) and predicted (curve) PDF's of local normalised maxima. The prediction is based on expression (10).

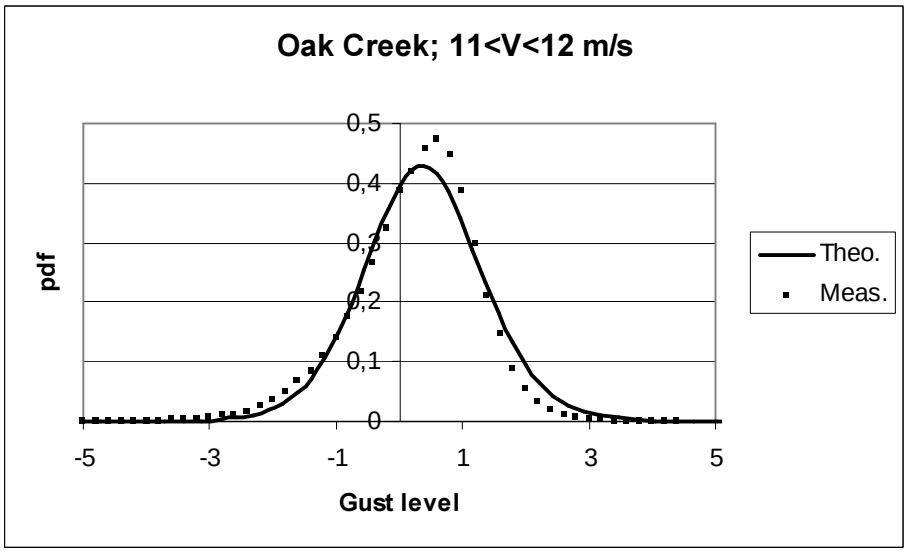

Figure 5-62 Estimated (squares) and predicted (curve) PDF's of local normalised maxima. The prediction is based on expression (20).

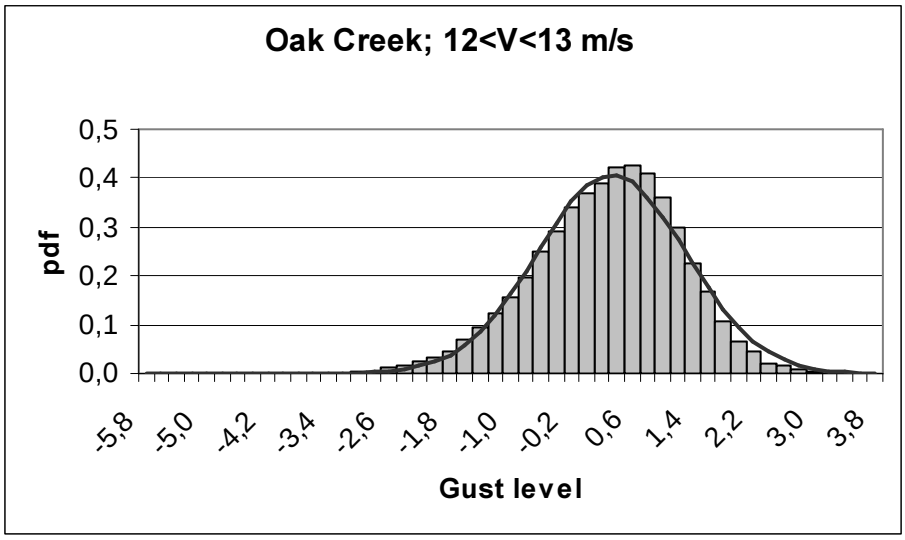

Figure 5-63 Estimated (histogram) and predicted (curve) PDF's of local normalised maxima. The prediction is based on expression (10).

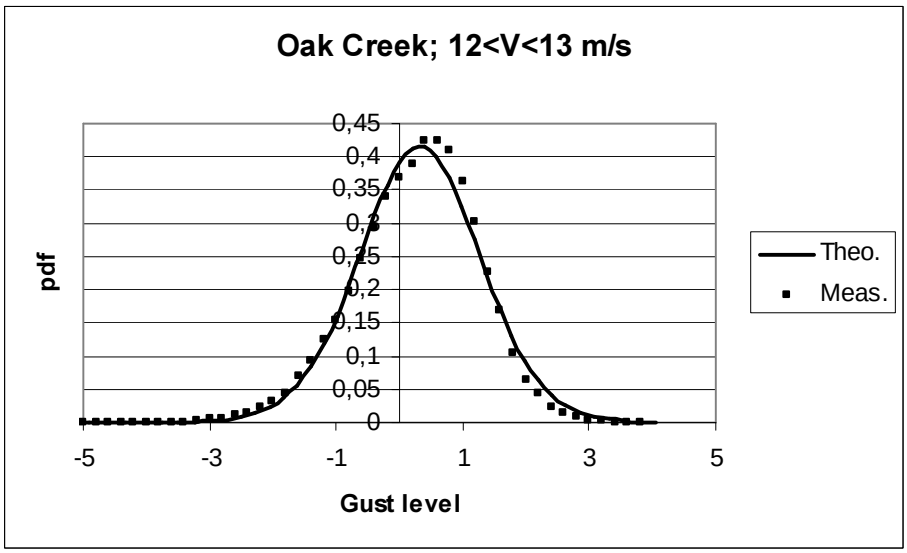

Figure 5-64 Estimated (squares) and predicted (curve) PDF's of local normalised maxima. The prediction is based on expression (20).

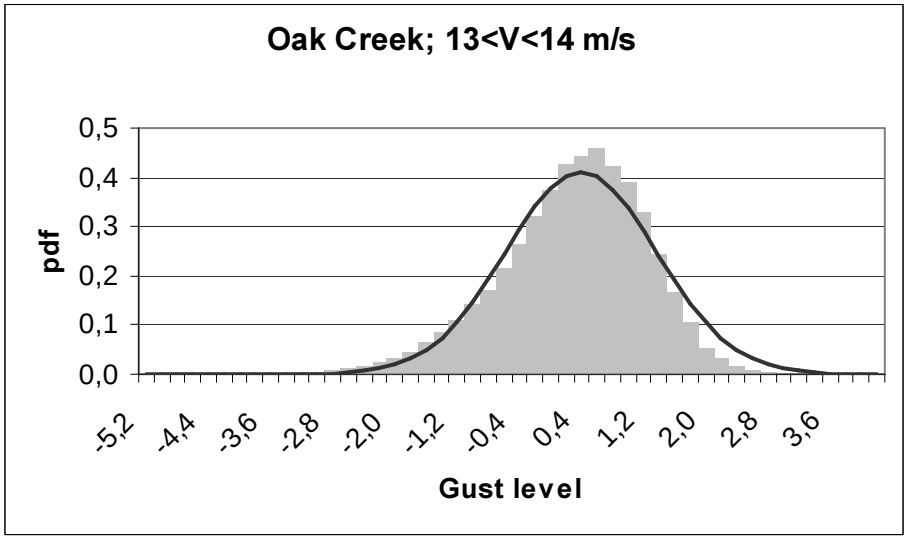

Figure 5-65 Estimated (histogram) and predicted (curve) PDF's of local normalised maxima. The prediction is based on expression (10).

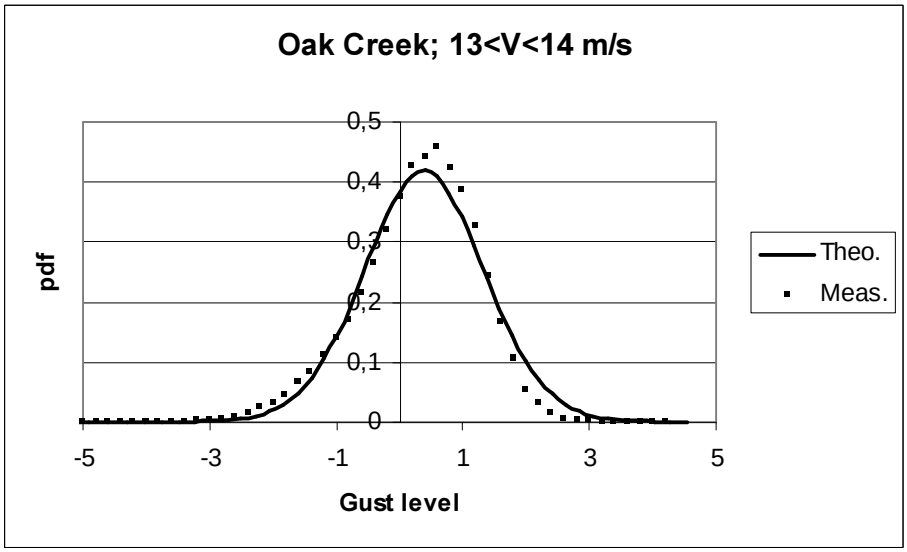

Figure 5-66 Estimated (squares) and predicted (curve) PDF's of local normalised maxima. The prediction is based on expression (20).

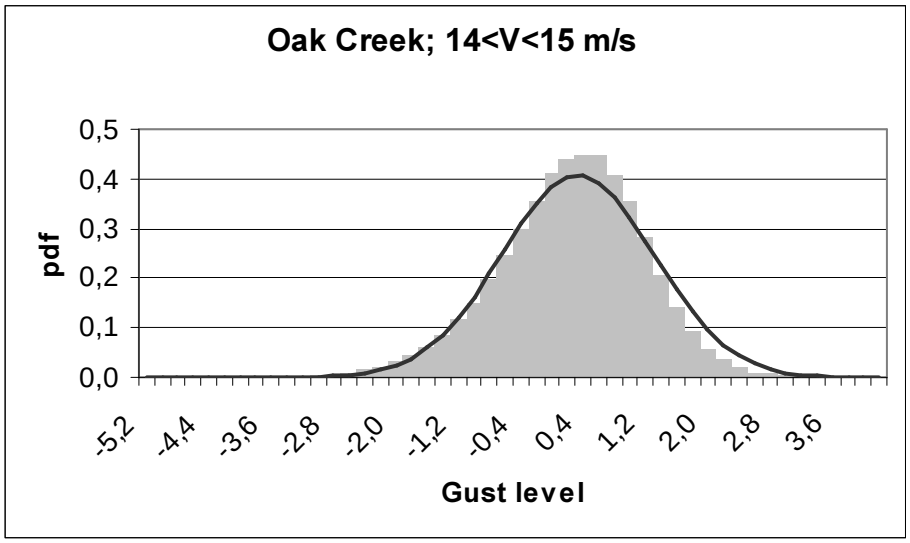

Figure 5-67 Estimated (histogram) and predicted (curve) PDF's of local normalised maxima. The prediction is based on expression (10).

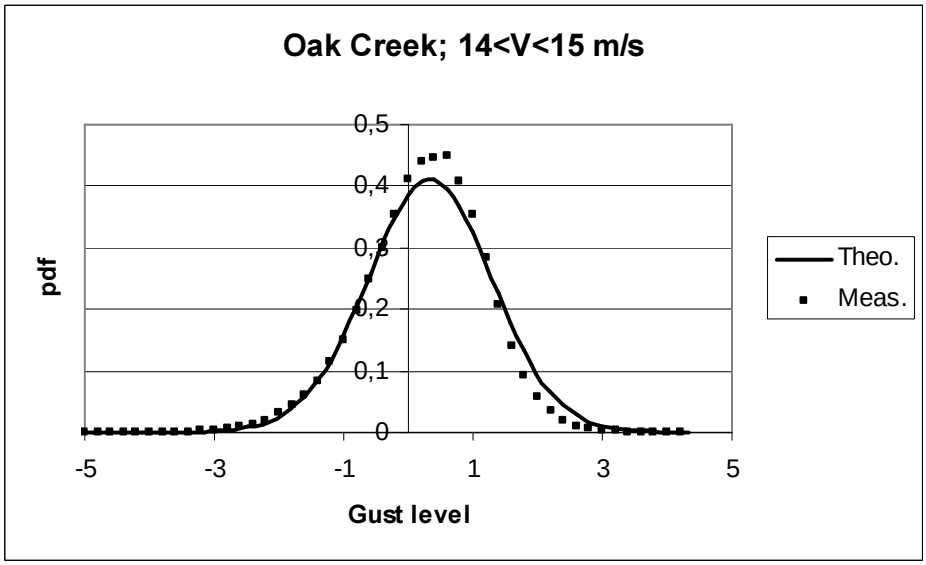

Figure 5-68 Estimated (squares) and predicted (curve) PDF's of local normalised maxima. The prediction is based on expression (20).

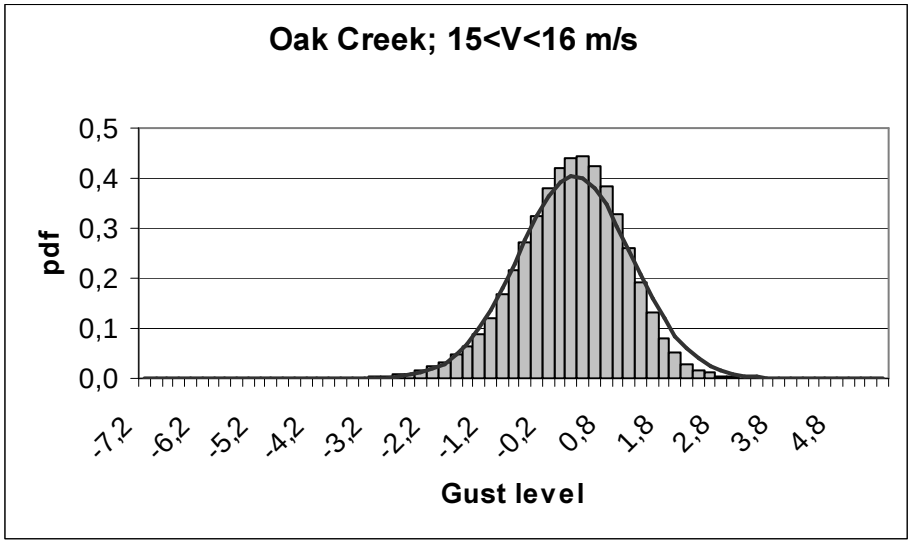

Figure 5-69 Estimated (histogram) and predicted (curve) PDF's of local normalised maxima. The prediction is based on expression (10).

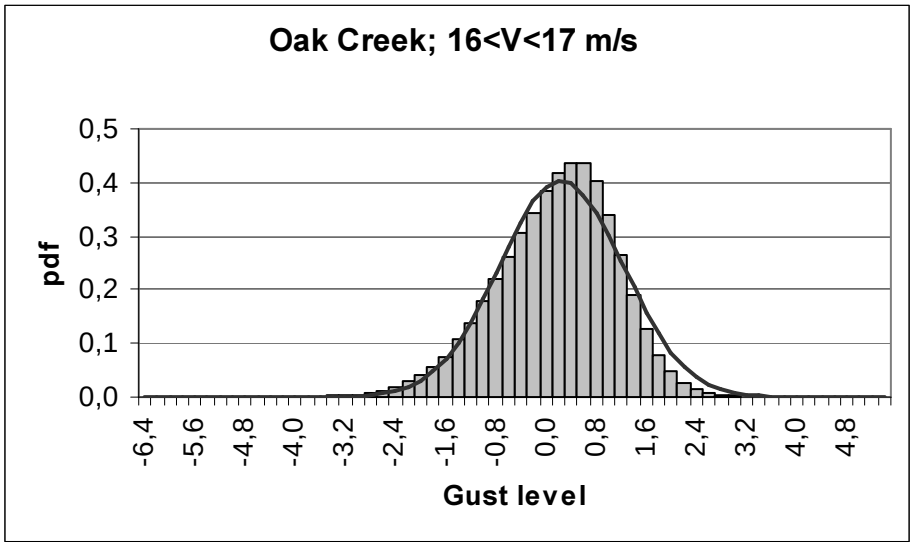

Figure 5-70 Estimated (histogram) and predicted (curve) PDF's of local normalised maxima. The prediction is based on expression (10).

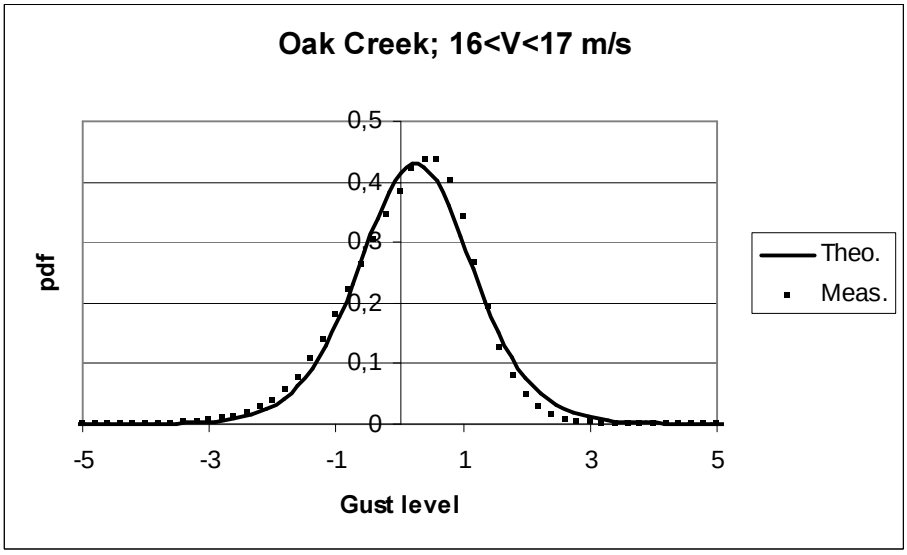

Figure 5-71 Estimated (squares) and predicted (curve) PDF's of local normalised maxima. The prediction is based on expression (20).

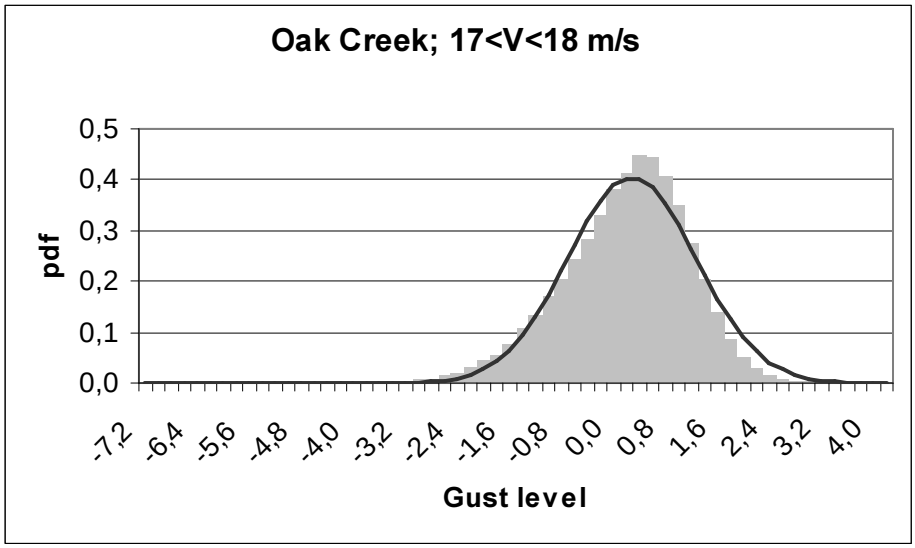

Figure 5-72 Estimated (histogram) and predicted (curve) PDF's of local normalised maxima. The prediction is based on expression (10).

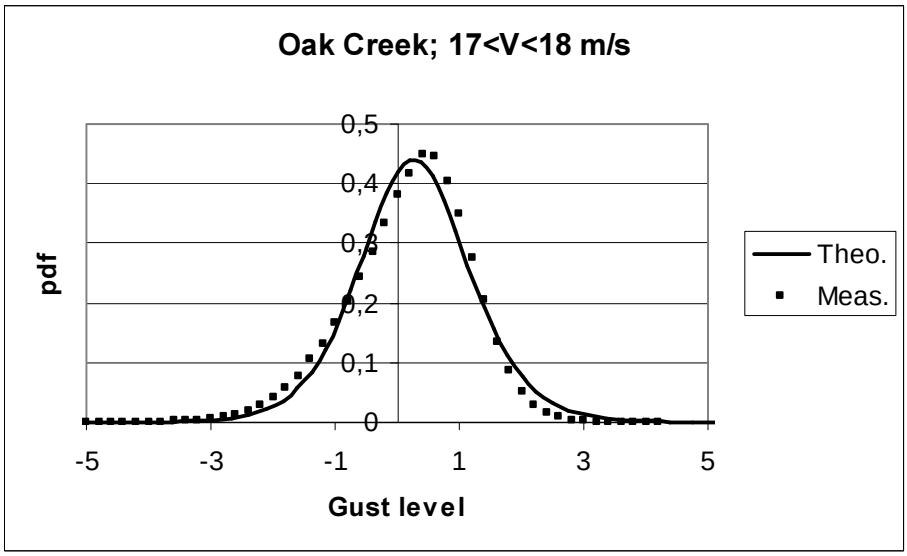

Figure 5-73 Estimated (squares) and predicted (curve) PDF's of local normalised maxima. The prediction is based on expression (20).

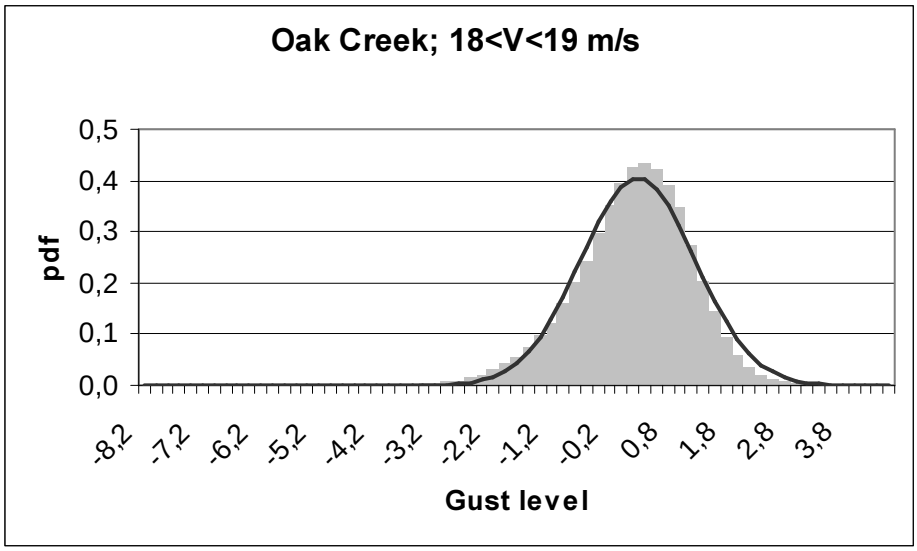

Figure 5-74 Estimated (histogram) and predicted (curve) PDF's of local normalised maxima. The prediction is based on expression (10).

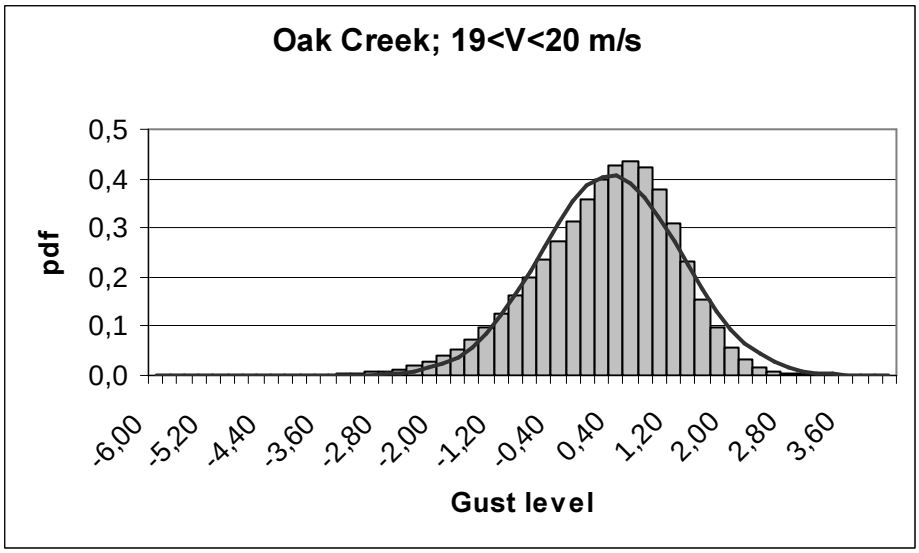

Figure 5-75 Estimated (histogram) and predicted (curve) PDF's of local normalised maxima. The prediction is based on expression (10).

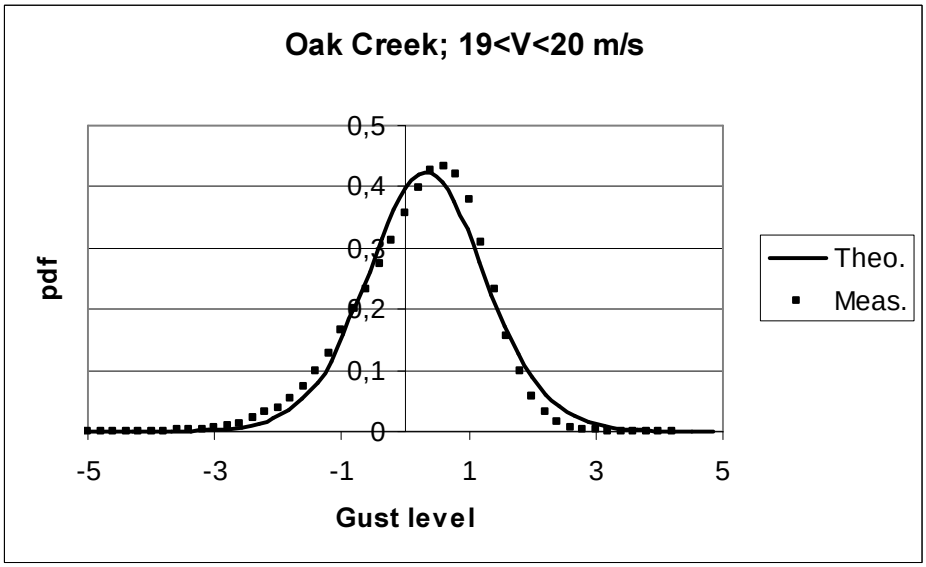

Figure 5-76 Estimated (squares) and predicted (curve) PDF's of local normalised maxima. The prediction is based on expression (20).

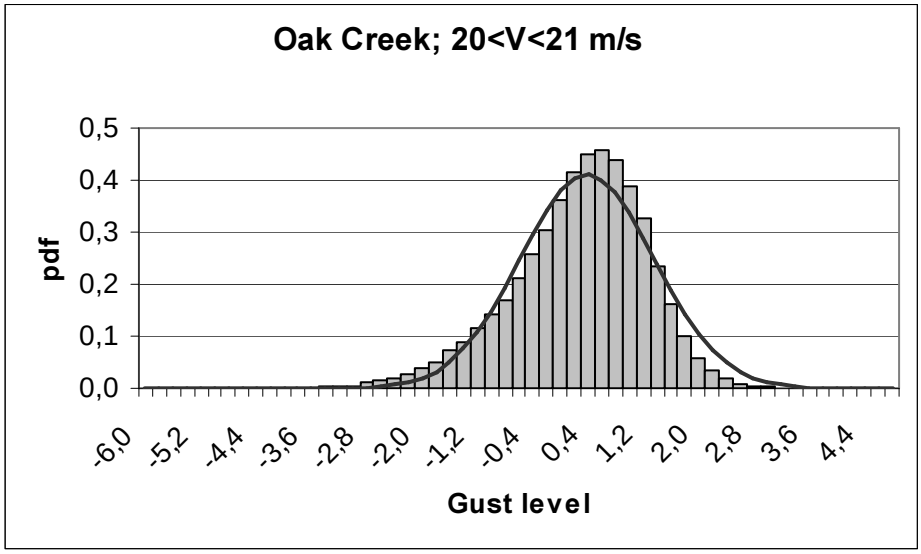

Figure 5-77 Estimated (histogram) and predicted (curve) PDF's of local normalised maxima. The prediction is based on expression (10).

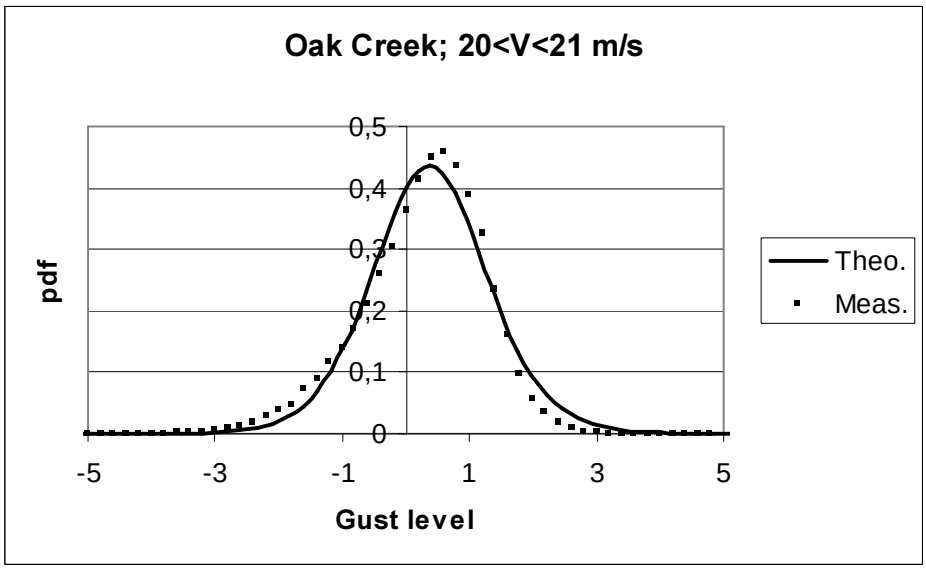

Figure 5-78 Estimated (squares) and predicted (curve) PDF's of local normalised maxima. The prediction is based on expression (20).

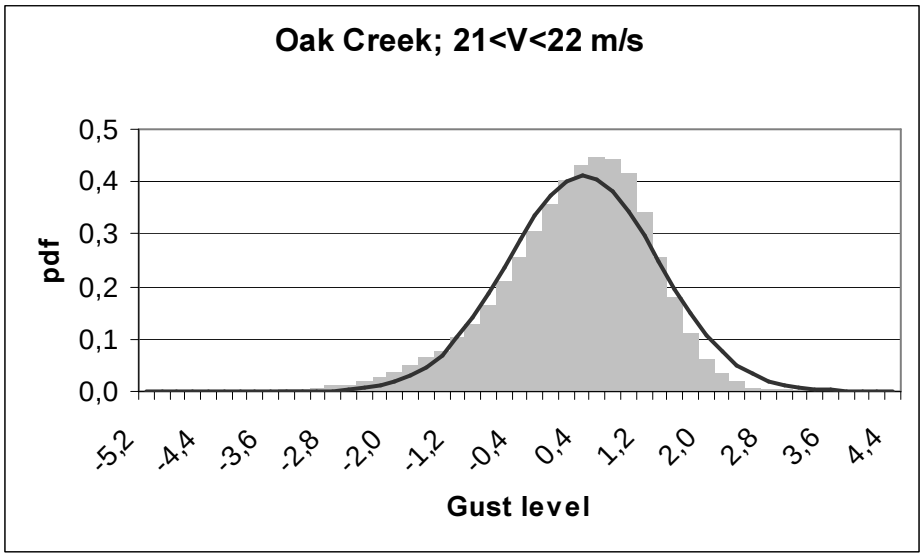

Figure 5-79 Estimated (histogram) and predicted (curve) PDF's of local normalised maxima. The prediction is based on expression (10).

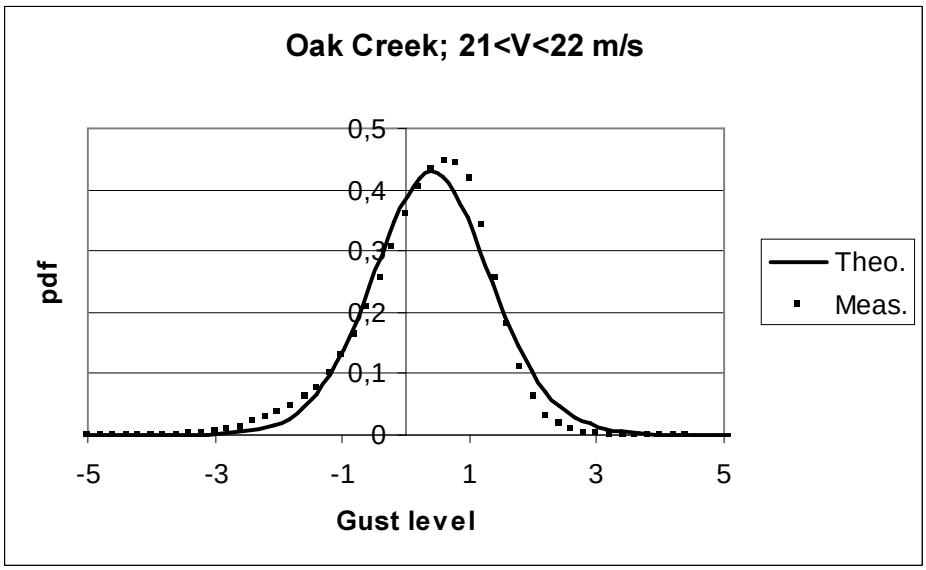

Figure 5-80 Estimated (squares) and predicted (curve) PDF's of local normalised maxima. The prediction is based on expression (20).

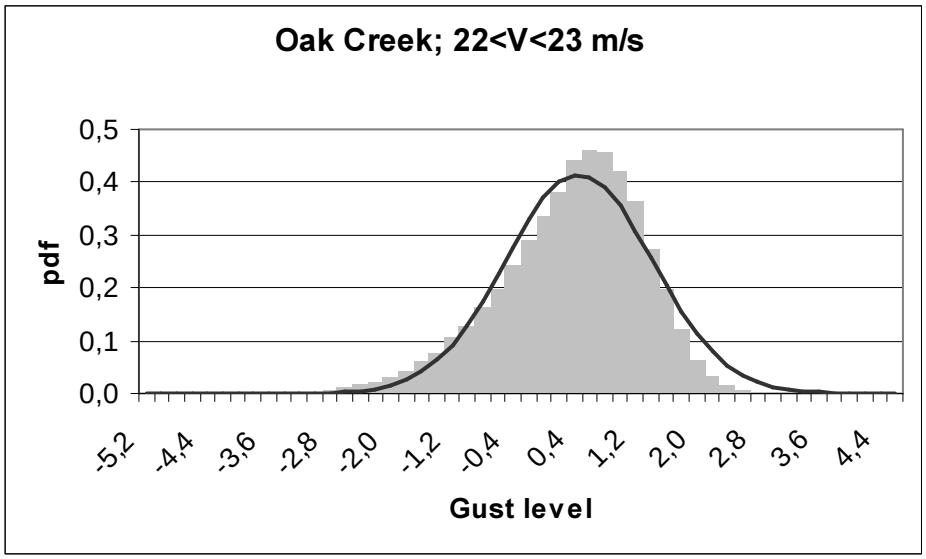

Figure 5-81 Estimated (histogram) and predicted (curve) PDF's of local normalised maxima. The prediction is based on expression (10).

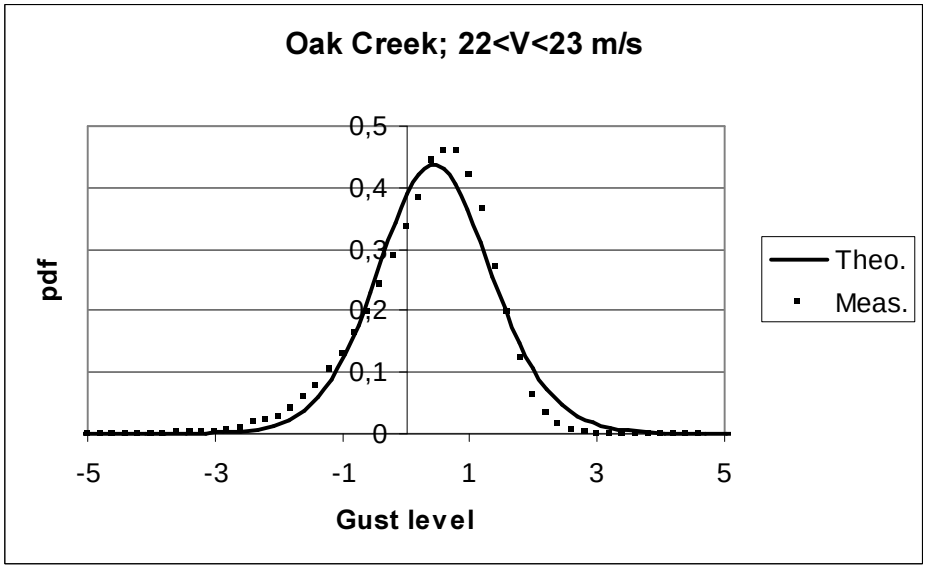

Figure 5-82 Estimated (squares) and predicted (curve) PDF's of local normalised maxima. The prediction is based on expression (20).

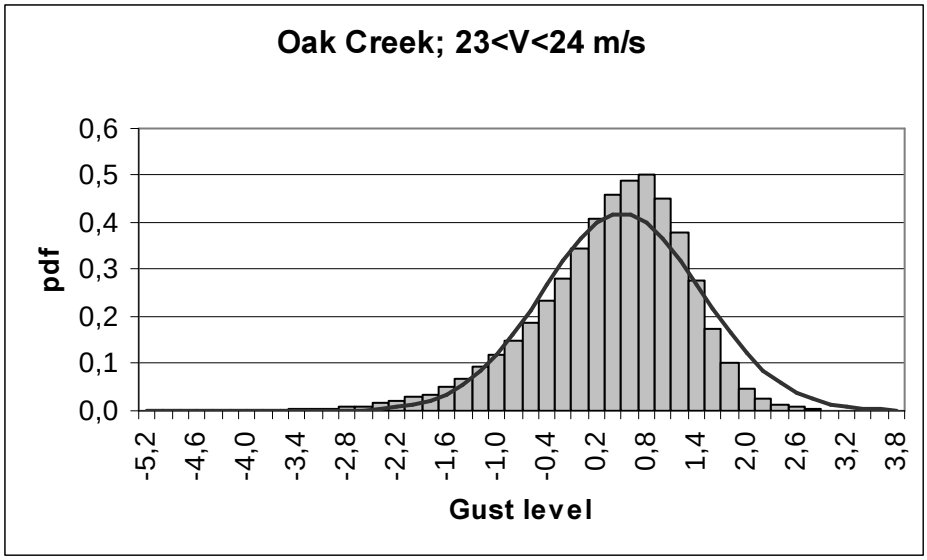

Figure 5-83 Estimated (histogram) and predicted (curve) PDF's of local normalised maxima. The prediction is based on expression (10).

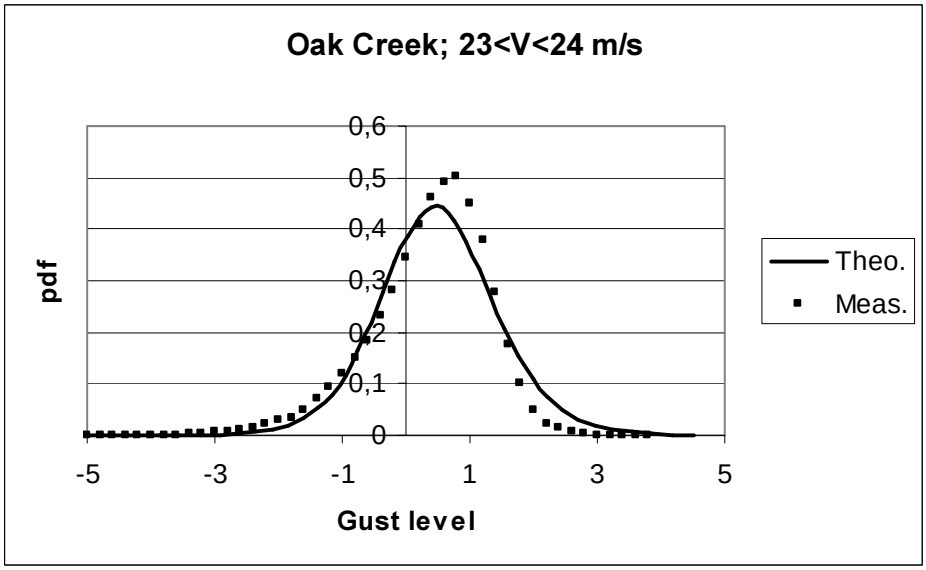

Figure 5-84 Estimated (squares) and predicted (curve) PDF's of local normalised maxima. The prediction is based on expression (20).

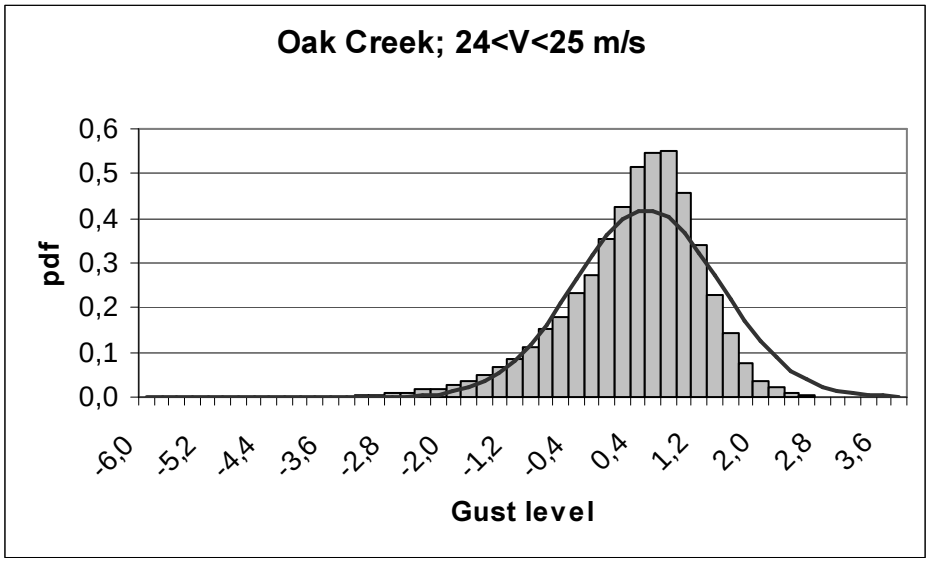

Figure 5-85 Estimated (histogram) and predicted (curve) PDF's of local normalised maxima. The prediction is based on expression (10).

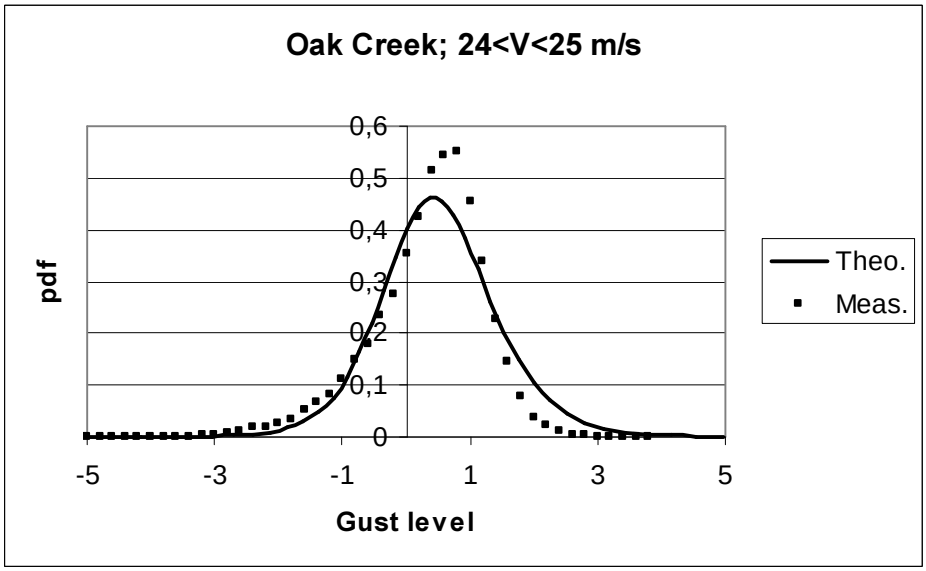

Figure 5-86 Estimated (squares) and predicted (curve) PDF's of local normalised maxima. The prediction is based on expression (20).

The local maxima statistics of the Oak Creek data differ somewhat from the statistics of maxima related to the other three investigated sites. The deviation is believed to be caused by the fact that the wind speed time series from this complex site in general do not represent Gaussian turbulence.

As expected, the predictions based on expression (20) have a better performance than the predictions based on relation (10). The predicted PDF's based on (20) are seen to fit fairly good with the estimated PDF's determined by direct counting in the measured data. However, especially for mean wind speed bins that exhibits large deviations from a Gaussian behaviour, considerable discrepancies result.

This deviation may be partly due to the fact that expression (20) is based on an asymptotic Hermite expansion truncated after three terms. The performance may be improved by including more terms in the expansion. An other, and maybe more essential, explanation is that that the predictions according to (20) is based on *mean* skewness and kurtosis of all wind speed time series associated with the particular bin. However a considerable spread of these values is observed within each wind speed bin. As an example, the distribution of skewness and kurtosis is shown for the wind speed time series with mean wind speeds in the range [23m/s;24m/s] in Figures (5-87) and (5-88).

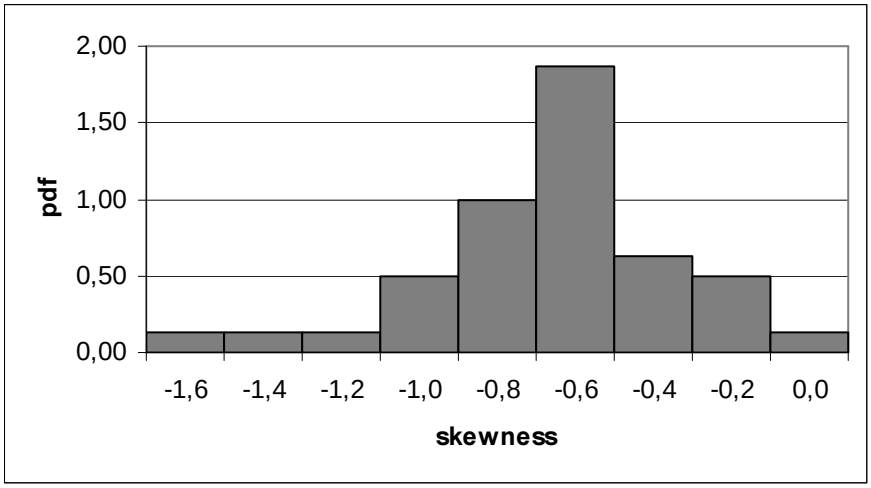

Figure 5-87 Distribution of skewness associated with time series with mean wind speeds in the range [23m/s;24m/s].

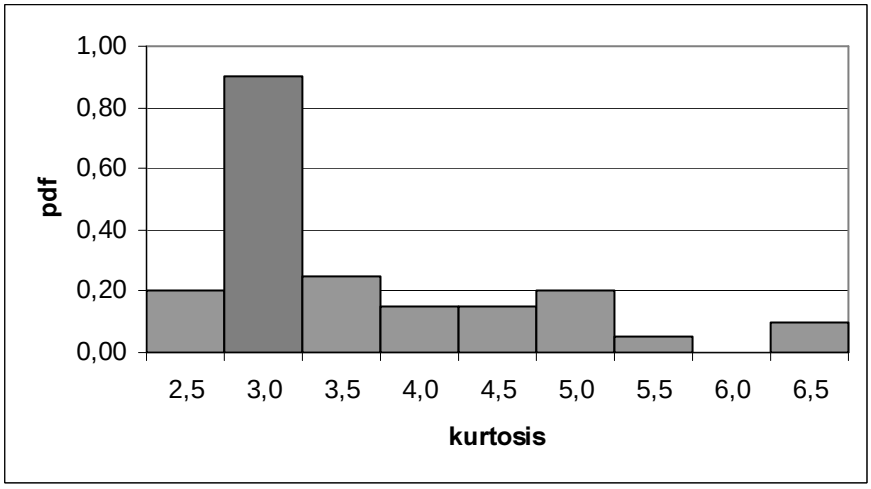

Figure 5-88 Distribution of kurtosis associated with time series with mean wind speeds in the range [23m/s;24m/s].

Note, that when deviations occur, the predictions according to expression (20) is always conservative in the sense that the predictions tend to overestimate the probability of the large local maxima (that is the most critical for the structural reliability).

The bandwidth parameter associated with these data depends somewhat on the mean wind speed. The bandwidth parameter is in the range 0.90 to 1.00, with a tendency of decreasing bandwidth with increasing mean wind speed. However, all observed values of the bandwidth parameter indicate broad-banded signals.

6. Conclusions

The statistics of local wind speed extremes (maxima) has been investigated. The investigation has comprised a theoretical study and a subsequent verification of the findings from this study by comparing the theoretical predictions with analysis of data representing different types of stochastic processes.

The detailed verification has been performed by comparing model predictions to analysis of both synthetic fields and full scale wind field measurements. The synthetic fields have encompassed both narrow banded stochastic processes (wave simulations) and broad banded stochastic processes (wind simulations). All synthetic processes were ideal Gaussian processes. The full scale stochastic processes were represented by (broad-banded) wind measurements. Both Gaussian and non-Gaussian processes have been analysed.

The verification has shown exceptional good agreement between the predictions and the estimates based on direct analysis of the involved time series when the underlying stochastic process is Gaussian or close to Gaussian. This is true for narrow banded as well as for broad banded signals.

For stochastic time series with a deviation from a Gaussian behaviour, the theoretical predictions in general still fits well with the estimated PDF's estimated based on direct counting in the measured data. However, for very pronounced deviations from the Gaussian behaviour some deviations between predictions and analyse results has been observed. However, these deviations is conservative in the sense that the predictions tend to overestimate the probability of large local extremes (which is most critical for the structural reliability).

7. References

1. Dragt, J.B. and Bierbooms, W. (1996). Modelling of Extreme Gusts for Design Calculations. EUWEC'96, Göteborg, 20-24 May.

2. Draft IEC 61400-1, Ed. 2 (1998). Wind Turbine generator Systems - Part 1: Safety Requirements. International Electrotechnical Commission (unpublished).

3. Bierbooms, W. (2000). Development of an advanced method to determine the dynamic response of a wind turbine on extreme gusts (work package 3 *New*Gust).

4. Larsen, G.C., Bierbooms, W. and Hansen, K.S. (2003). Mean Gust Shapes. Risø-R-1133(EN).

5. Rice, S.O. (1958). Mathematical analysis of random noise, Bell Syst. Techn. J., 23 ('44); Reprinted in N. Wax (ed.), Selected papers on noise and stochastic processes, Dover Publ..

6. Cartwright, D.E. and Longuet-Higgins, M. S. (1956). The statistical distribution of the maxima of a random function, Proc. Royal Soc. London Ser. A 237, 212-232.

7. Winterstein, S.R. (1988). Nonlinear Vibration Models for Extremes and Fatigue. Journal of Engineering Mechanics, ASCE, Vol. 114, No. 10, pp. 1772-1790.

8. Bierbooms, W. (1998). *SWING4 User Guide*, IW-98133R, Delft University of Technology.

9. "Database on Wind Characteristics". http://www.winddata.com/

Bibliographic Data Sheet **Risø-R-1220(EN)**

Title and authors

Statistics of Local Extremes

Gunner Chr. Larsen, Wim Bierbooms and Kurt S. Hansen

ISBN
87-550-2777-6; 87-550-2778-4 (Internet)

ISSN
0106-2840

Department or group
Wind Energy Department

Date
December 2003

Groups own reg. number(s)
1110020-00

Project/contract No(s)
JOR3-CT98-0239

Pages	Tables	Illustrations	References
60	4	89	9

Abstract (max. 2000 characters)

The gust events described in the IEC-standard are formulated as coherent gusts of an inherent deterministic character, whereas the gusts experienced in real situation are of a stochastic nature with a limited spatial extension. This conceptual difference may cause substantial differences in the load patterns of a wind turbine when a gust event is imposed.

The Newgust method is a rational way of taking wind speed gust situations into account in a design process. A corner stone in the method is a cogent algorithm to embed a wind speed gust of a prescribed appearance in a stochastic wind field [Dragt, 1996]. However, dealing with wind turbine design, not only detailed knowledge on the spatial/time structure of the gust event is required. The probability of occurrence of a gust event with a given wind speed amplitude/magnitude is equally important. This theme is addressed in the present report.

A theoretical expression for the probability density function associated with local extremes of a stochastic process is presented. The expression is basically based on the lower four statistical moments and a bandwidth parameter. The theoretical expression is subsequently verified by comparison with simulated synthetic wave/wind fields as well as with measured wind fields covering a broad range of mean wind speed situations and terrain conditions. The simulated wave fields represents narrow band processes, whereas the wind fields represent broad-banded processes.

The work reported makes part of the project “Modelling of Extreme Gusts for Design Calculations ” (NEWGUST), which is co-funded through JOULEIII on contract no. JOR3-CT98-0239.

Descriptors INIS/EDB

DATA ANALYSIS; PROBABILITY; STOCHASTIC PROCESSES; STORMS; VELOCITY; WIND; WIND TURBINES